CHAPTER I

OVERVIEW

1.1 INTRODUCTION

The utilization of solar technologies requires the development of materials that can be used to make this source of energy cheap and reliable. One such need involves the development of transparent conducting solid thin films that are spectrally selective. Spectral selectiveness is an important property in solar cells because the spectrum of interest for this application is restricted to the visible and near infrared region and so the unwanted wavelength regions must be selectively rejected. This research focuses on producing transparent conducting thin films of zinc and aluminium oxides which are characterized and modeled for efficient solar energy applications in thin film solar cells and other solar energy systems. The choice of zinc and aluminium oxides is based on the fact that they are locally available in Zambia and can be obtained cheaply as opposed to indium tin oxide (ITO) which is expensive and rarely available.

Thin film solar cells (TFSC) are a good choice in terms of the device design and fabrication process and offer an interesting alternative to p-n junction silicon (Si) based photovoltaic (PV) devices. In principle, a solar cell is a junction device which is made of two electronically non similar materials separated by a thin electronic barrier which acts as a dividing line for charge. The functions of each component of a TFSC device in figure 1.1 [1] are discussed. A TFSC is comprised of several layers of different thin film materials. It is typical that a cell is made up of a substrate, a transparent conducting

oxide (TCO), a window layer, an absorber layer and a metal contact layer all of which have different physical, chemical, optical and electronic properties. Individual properties of the cell components each affect the overall performance of the cell. With this in mind, it is important to understand the behavior of these solar cell components.

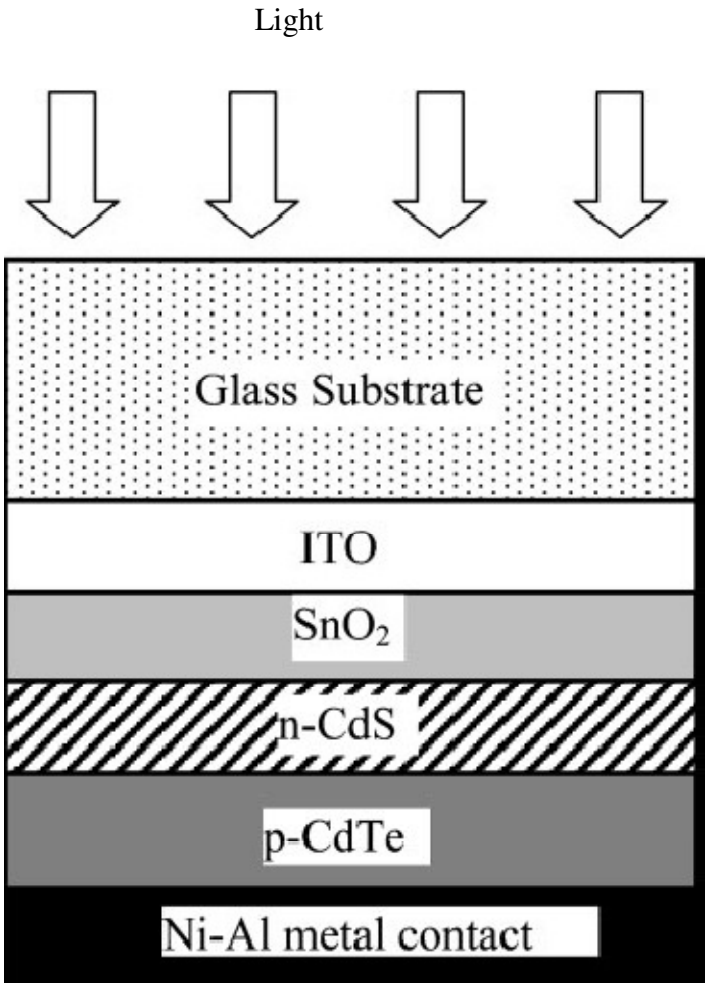

Figure 1.1 Typical structure of a single p-n junction thin film solar cell.

The first layer of the solar cell in figure 1.1 is the substrate. A substrate is a passive component of a cell which is basically used as a surface upon which the film coating is

done. It is required to be mechanically stable and inert during film coating. For the configuration in figure 1.1, the substrate is required to be transparent to the incident light. This is the reason why glass substrates were chosen. In applications other than thin film solar cells, a substrate could be a metal, a metallic coating on glass or a polymer wafer.

The next two layers of the solar cell are transparent conducting oxides (TCO). Their main function is to transmit the wanted visible and near infrared electromagnetic waves to the absorber layer where conversion to holes and electrons takes place, but to filter out unwanted infrared and ultraviolet (UV) wavelengths which would cause the solar cell to overheat and hence reduce its efficiency. This filtering is called spectral selectivity. These layers are therefore spectral selective layers of the solar cell. Two layers were used to improve the filtering of the unwanted wavelengths, i.e., it improves the spectrally selectivity. The TCOs also function as one of the contacts of the circuit. The other contact is the Ni-Al layer. The TCOs also contribute to the conversion of light to charge carriers to a small extent, the main conversion being done in the absorber layer described below.

Our focus in this study is on the TCOs. Transparent conducting oxides are generally n-type semiconductor metal oxides which exhibit high transmittance of the visible (VIS) and near infrared (NIR) radiation and have high conductivity for efficient charge carrier transport when used as thin film electrodes or contacts in solar cells. It is important that

TCOs have high transparency in the solar region and high electrical conductivity because enough light must be allowed to pass through them onto the absorbing layer; since they form one electrical contact of the solar cell, they must be good conductors. Uniformity of the film surface is an important property that TCOs must have. This has a direct bearing on the film sheet resistance and hence the conductivity. They are coated on a substrate as shown in figure 1.1. In this cell structure, an indium doped tin oxide (ITO) and tin oxide (SnO_2) ITO/SnO_2 transparent conducting oxides bi-layer were used. TCOs ensure that most of the incident light is transmitted to the active absorber layer of the cell. They also ensure that infrared radiation is reflected so that it does not cause heating in the cell because this would degrade the cell's performance. Since current ITO materials are very expensive, we propose the use of Zinc Oxide doped with aluminium (ZnO:Al) as a cheaper alternative which provides the same transparency in the VIS-NIR spectra as ITO. Further, we propose the use of aluminium oxide doped with zinc (Al_2O_3:Zn) as another TCO which should form a bi-layer with ZnO. These proposed oxides have been produced and characterized for the purpose of improving the performance of the cell in the region where they are applied.

The fourth and fifth layers form the p-n junction which is the heart of the solar cell. The overall function of these layers is to create a potential difference to drive the charge carriers through the circuit. The fourth layer, which in our case is n-CdS, is required to allow the light transmitted through the TCOs to pass to the fifth layer; hence it is called the window layer. The fifth layer is the absorbing layer, which in our case is p-CdTe. It

is in this absorbing layer that most of the conversion of light to charge carriers takes place.

Once created, the electrons and holes require a potential difference to flow. The function of the fourth layer, by making contact with the fifth layer, is to provide this potential difference. At the same time the fourth layer must not prevent light from reaching the fifth absorbing layer.

Cadmium sulfide (CdS) is often used in copper indium gallium diselenide (CIGS) solar cells as a window layer. The absorber layer is made of a material which absorbs most of the incident photons and generates an electric current. Copper indium gallium diselenide and cadmium telluride (CdTe) are some of the common materials used.

The sixth layer is a metal contact, which together with the TCOs connects the solar cell to the external circuit. In the illustrated example, a nickel-aluminium (Ni-Al) metal contact has been used.

There have been important developments in the utilization of solar energy in the recent past through improvements made to solar cells, solar thermal collectors (collectors designed to collect heat by absorbing sunlight) and other solar application devices. However, the biggest challenge in making solar energy cheaper and reliable lies in the development of effective and efficient solar energy materials for both thermal and

photovoltaic applications. The main objective of this research is to address the problem of the high production cost of solar cells by producing, characterizing and modeling cheaper TCOs as a starting point. We investigate cheaper options for transparent conducting oxides which should replace the rare and expensive TCOs currently in use such as ITO. Further, we employ a fabrication process that brings the cost of solar cell production down and offers a chance for large surface coating of thin films. The use of ZnO and Al_2O_3 transparent conducting oxides is not new in this area of research. However, the mutual doping of the two: ZnO doped with aluminium (ZnO:Al) and aluminium oxide doped with zinc (Al_2O_3:Zn) is a new and novel approach. It is a new innovation to have a combination of mutually doped zinc and aluminium oxides making a bi-layer in a solar cell and acting as the transparent oxides replacing the ITO/SnO_2 combination used in a typical solar cell, as shown in figure 1.1. In addition, a locally constructed and tailor-made spray pyrolysis unit has been used in the coating of these thin films. Further, standard analytical techniques of characterization have been used. These are spectrometry, profilometry and electrical characterization using a four point resistance probe. The Maxwell-Garnett and Bruggeman effective medium theories have been applied in modeling the optical properties of the films.

Recent years have seen the importance of energy being brought into sharp focus as world economies continue to grow amidst spiraling international prices for conventional sources of energy such as petroleum, coal and hydro electricity. Despite the 2008-2009 world economic meltdown, the demand for energy still remains high, thus creating a

general sense of energy crisis. The way to mitigate the crisis is to turn to clean and less costly renewable sources of energy of which solar energy has the best potential.

Renewable energy sources are being increasingly used but their contribution to total energy supply still remains low [2]. The available renewable energy sources include wind, solar, geothermal, bio-fuel and hydro power. Wind energy finds its applications in water pumping for household use and irrigation with a possibility of electricity generation in areas where wind speeds exceed 5 m/s [3]. Geothermal energy is constrained by the limited presence of hot springs and where they exist; their exploitation is limited except in very few cases. While hydroelectricity ranks high in importance as a source of energy, it faces the challenge of limited installed capacity and high running costs, which make it unaffordable to poor families and inaccessible to people in remote settlements. We have seen wide spread shortages of hydro electric power leading to repeated power cuts and load shedding in Zambia and also other countries in Southern Africa Development Community (SADC) countries. The same trend has been recorded in many other parts of the world. All this has been as a result of energy demand overriding supply. There remains hope of improvement in the situation due to the fact that solar energy technologies are rapidly developing. The energy shortages presently being experienced and those projected in the near future could be averted with fully developed clean solar technologies. This is the reason why in the world today we have to think of solar as a reliable alternative and give it the attention that it deserves.

1.2 SPECTRAL SELECTIVITY

Radiation prevalent in our environment has appreciable variance in spectral properties. In particular, solar radiation has a wide range of wavelengths spanning from the ultraviolet to the infrared [4]. Figure 1.2 on page 10 gives the spectra for (a) ideal blackbody radiation, (b) extraterrestrial solar radiation, (c) atmospheric absorption and (d) the human eye and green algae sensitivities. We see from figure 1.2 (a) and figure 1.2 (b) that the solar and infrared spectra do not overlap because they have specific wavelength ranges. This means that by use of spectrally selecting materials, we can work with specific regions of the spectrum in a given wavelength range and avoid unwanted radiations. This is important because different applications such as solar cells, solar thermal collectors, optical filters and biophysical systems use different parts of the electromagnetic spectrum. In the case of solar cells, we are interested in the visible and near infrared wavelength region. On the other hand, transmission of the IR is more important in solar thermal collectors and solar water heating systems. The most important part of the solar irradiation is that which reaches the surface of the earth. A look at part (c) of figure1.2 gives us a picture of a typical absorption spectrum for clear weather conditions across a vertical stretch of the atmosphere. This figure can be viewed in three sections of the spectrum. In one part, we see maximum absorption of shorter wavelength UV region. This is followed by a high luminous or light transmission in the wavelength region lying between 300 nm and 800 nm. The third band exhibits a complicated absorption and transmission profile for wavelengths in the range 800 nm < λ < 1300 nm. The high absorption sections can be attributed to the presence of atmospheric elements such as water vapour, carbon dioxide and ozone, which tend to

absorb or scatter the radiation falling on them. These high absorption regions are intertwined with sections of high transmission. Beyond 1300 nm we obtain maximum attenuation. Part (d) of figure 1.1 gives the implications for biophysical systems as regards solar transmission. The human eye, as is obviously expected, has a higher relative spectral sensitivity at the peak of the luminous solar spectrum at wavelength 555 nm whereas photosynthesis in plants and green algae is more efficient in the neighbourhood to the right. Therefore, much of plant photosynthesis activity is favoured in the NIR radiation range. This trend of photon efficiency in the infrared is relevant for greenhouse applications.

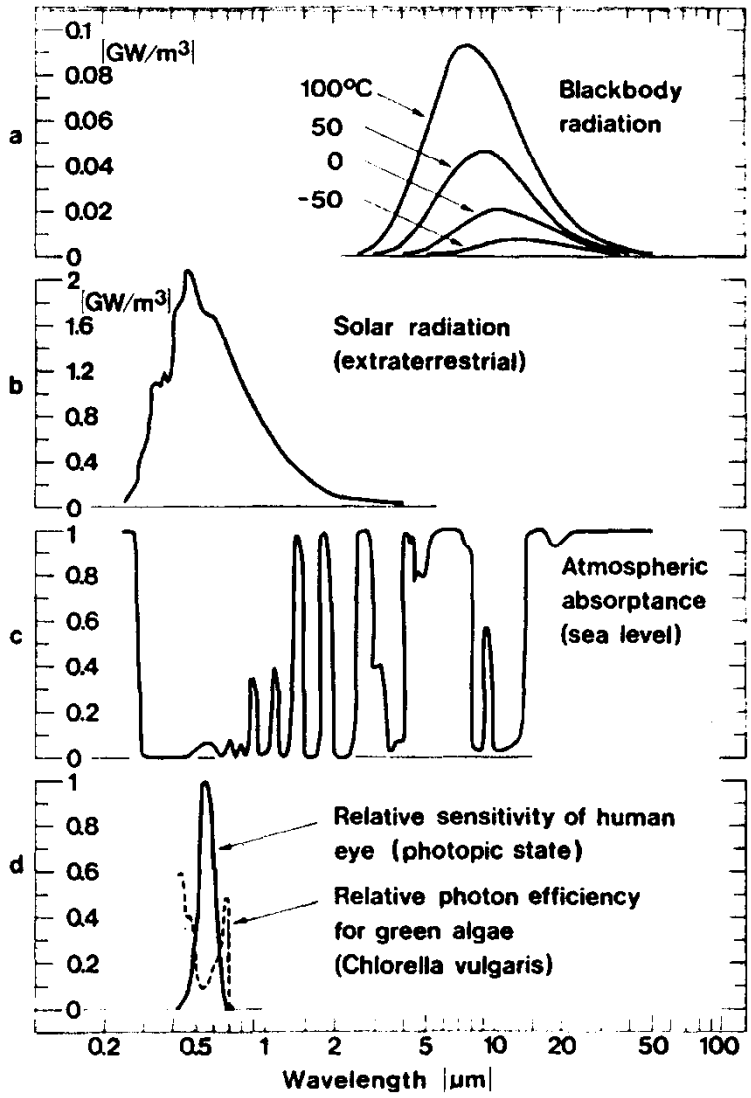

Figure 1.2 Spectral curves a) blackbody radiation for four different temperature values, b) extraterrestrial solar radiation, c) absorption spectrum across the full atmospheric envelope at clear weather conditions, d) human eye sensitivity (thick line) and relative photon efficiency for plants and green algae [5].

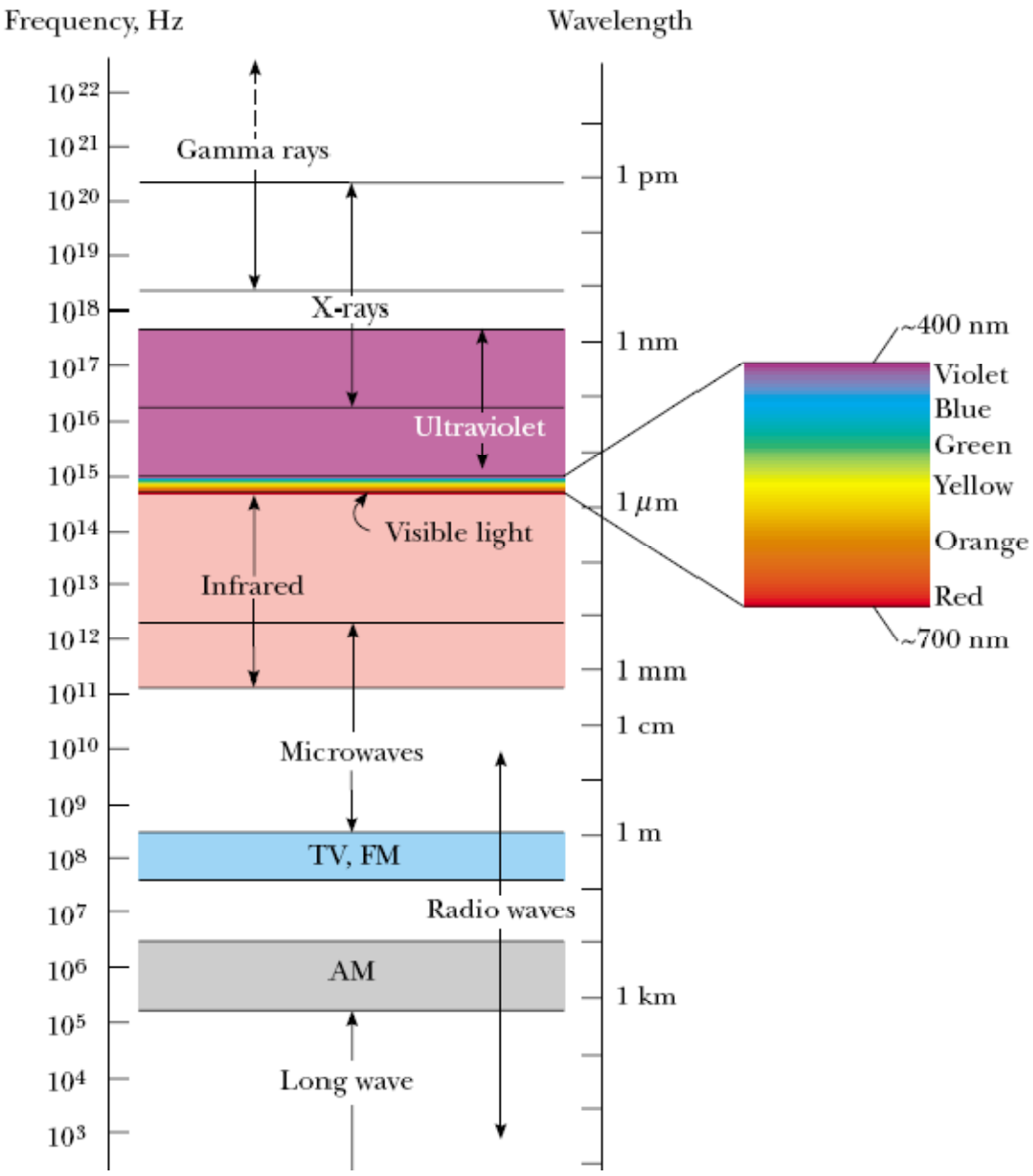

Figure 1.3 The electromagnetic spectrum [6].

Figure 1.3 on page 11 shows the entire electromagnetic (EM) spectrum. The section of the spectrum of interest, as far as solar energy applications are concerned, lies in the

wavelength range 0.3 μm -100μm. This defines mostly the UV-VIS and NIR regions of the spectrum as opposed to far infrared.

As a result of these spectral differences, thin films can be made that selectively absorb or transmit in one region of the spectrum while reflecting in the others. We call such surface coatings spectrally selective coatings. For purposes of solar luminance, one is expected to use thin films that have high transmission in the solar spectrum. High absorption in the infrared region is expected of films that are used in thermal applications.

1.3 MATERIAL CHOICE AND ASSOCIATED PROPERTIES

Spectral selectiveness of various materials to be used for thin films has been studied by many researchers. Semiconductors have been found to yield good transparent coatings [7]. It is a known fact that the usefulness of a transparent conductor lies in its optical transmission and electrical conductivity. Haake [8] has described both metal and semiconductor thin film materials. Metal thin films have two major drawbacks which make them unsuitable for use in transparent conducting materials. The two drawbacks are high sheet resistance and high optical reflectance losses. Metals are also opaque. However, electrical and optical bulk properties suitable for transparent electrodes are evident in gold, copper and silver. Materials with high carrier mobility and low effective carrier mass are good for transparent conductors. This is because the generation of an electric current in a solar cell depends on carrier mobility. The transmission region of

semiconductors is restricted to wavelengths longer than the materials band-gap energy ($E_g > 3eV$) [8].

We now discuss the properties of various candidate materials for thin film coating are discussed one at a time. Each material presents its merits and demerits and why one can be preferred for use over the other. Indium tin oxide (ITO), cadmium oxide (CdO), tin oxide (SnO_2), Zinc oxide (ZnO) and aluminium oxide (Al_2O_3) are considered.

Indium tin oxide is outstanding material for transparent windows owing to its high transparency to solar radiation. Its main advantage lies in its outstanding optical and electronic properties which make it highly applicable in torch panel contacts, electrochromic and plasma displays, energy saving architectural windows, gas sensors, abrading layers, solar cells, transparent conducting and antireflection coatings as well as other applications [9-12]. ITO has a visible transmission greater than 80 per cent and an IR reflectance of about 80 per cent or greater. However, its low availability on the market and its high cost call for its substitution with other more readily available and cheaper materials.

Cadmium is another material that has been tried for transparent conductors and transmissions of 80-90 per cent have been recorded at $\lambda > 500$ nm. Cadmium oxide has not received much attention because of its transmission cut-off in its high conductivity state and also because of its low resistance against atmospheric moisture attack.

Yet another n-type material used and commercialized is tin oxide (SnO_2). It has acceptable electrical and optical properties and a band-gap of 3.5 to 3.93 eV with transmission in the visible region ranging between 80-85 per cent [13].

Another substance of interest is zinc oxide (ZnO) which has a melting point of 1975^{o}C and a specific gravity of 5.607 at 20^{o}C [14]. ZnO is a II-IV n-type semiconductor with a large band gap of 3.3 eV at room temperature. Experimental work has shown that zinc oxide is transparent to most of the solar spectrum and this makes it a good candidate as a transparent conducting oxide and a cheaper replacement for indium tin-doped oxide (ITO).

ZnO thin films get appreciation in their application as conducting and transparent window layers in amorphous silicon and copper indium selenium (CuInSe) based solar cells and as components in dye-sensitized solar cells (DSSCs). They are also used in acoustic wave filters, acoustic-optical and electro-optical devices, ultrasonic transducers and chemical sensors [15,16].

Aluminium oxide (Al_2O_3) thin films are grown using various techniques that include sputtering, chemical vapour deposition (CVD) and dip-coating techniques. The properties of the constituent metal oxide are favourable. The melting point of Al_2O_3 is 2045^{o}C. Thin films of Al_2O_3 have high transparency, high chemical stability, high electric insulation, high heat resistance, large mechanical strength and great hardness. They have a high dielectric constant of about 9 and can withstand high electric field

strengths. They are highly thermodynamically stable and have large band gap of 8.8 eV. The Al_2O_3 thin films are applicable as abrading and antireflection coatings and are favourable replacements for SiO_2 gate dielectrics in metal oxide semiconductor (MOS) devices. [17-20].

1.4 CHARACTERIZATION

Characterization is simply a process that seeks to single out or isolate the various properties associated with thin films. A successful and satisfactory characterization paves the way for possible uses of these materials in appropriate technological applications. In the case of this study, the optical, electrical and structural properties are investigated.

Researchers used many approaches to obtain these properties. In optical characterization, many have used spectrophotometers to measure transmittance, reflectance and absorption. Microstructure properties have been investigated using a wide range of techniques. These include, but are not limited to, transmission electron microscopy (TEM), scanning electron microscopy (SEM), atomic force microscopy (AFM) and Auger electron microscopy. Due to limited access these instruments, we have used only the AFM for micro-structural profiling. Film thickness was obtained by using the Tencor Alpha Step profiler. In certain coating processes, the thickness is determined in-situ. Determination of electrical properties is cardinal for coatings that are intended for applications in solar cells as this forms the basis for production of electricity. With this in mind, the film sheet resistance was determined using the four-

point resistance square probe. Resistance results can be processed to give resistivity and conductance of the thin films.

1.5 THIN FILMS

Thin films are employed in many high-technology industries for a wide range of applications. They are used in the manufacture of assorted technical products such as beam splitters, colour filters, narrow band pass filters, semi-transparent mirrors, polarisers, antireflection and transparent conducting coatings, absorber surface structures, reflection filters and so on. This underscores the importance of characterization of these films for applications in many optical, electrical and electronic devices. The parameters of special interest include film thickness, refractive index, resistivity and homogeneity of the surface spectral selectivity.

Thin film solar cells have the advantage that their production costs are promisingly low and that large scale production is feasible owing to the fact that new materials with excellent optical and electrical properties are being discovered and can be fabricated at relatively low cost. Furthermore, the deposition techniques for thin films are flexible and allow coatings for large surfaces. A large number of semiconductor metal oxides have been investigated and tried in the production of solar cells. The main parameters of interest are the performance efficiency and the durability of these cells [21].

In most polycrystalline or amorphous thin film solar cells, the active material is normally a semiconductor material coated on a suitable substrate, normally glass. The basic requirement is that the film thickness be greater than the inverse of the absorption coefficient of the material. This ensures that most of the light is absorbed [22].

1.6 MOTIVATION

Most of the work so far done on ZnO thin films employ growth methods other than spray pyrolysis. The common growth methods that are often employed in production of ZnO nanostructures include filtered vacuum arc deposition [23], reactive magnetron sputtering [24], pulsed laser deposition [25] and chemical vapour deposition (CVD) [26].

Reported research work on Al_2O_3 thin films has employed deposition methods that include electron beam deposition, reactive sputtering, magnetron sputtering and a few have used chemical vapour deposition. In this study however, we explore the spray pyrolysis deposition approach for both ZnO and Al_2O_3 thin films. This allows us to produce spectrally selective solid thin films using a convenient, reliable and cheap spray pyrolysis process of deposition, to investigate their optical and electrical properties and to theoretically model these properties in order to understand their nature and optimize them for applications in efficient solar energy structures.

CHAPTER II

THEORETICAL CONSIDERATIONS

2.1 SPRAY PYROLYSIS TECHNIQUES

Spray pyrolysis is one method of chemical vapour film deposition. It is a process in which an aqueous solution of metal oxides or halides is dispersed and transported by means of a carrier gas to a suitable substrate where a thin film forms. The process starts with production of small droplets of the precursor solution in the atomizer by way of a carrier gas pumped from a gas cylinder at controlled pressure by a system of pressure gauges. These droplets of the spray solution are transported by the carrier gas through a diffusion tube into the reaction chamber and onto a heated substrate where it immediately evaporates leaving a solid thin film. The temperature of the substrate is one of the key parameters that determine the final product and is therefore closely monitored. It is known that low temperatures result in cracked films whereas high substrate temperature produce ZnO films highly oriented in the (002) direction [27, 28]. In this particular setup the carrier gas used was nitrogen (N_2).

Spray pyrolysis is a simple and reliably cheap deposition process whose end result is determined by the following six parameters: temperature of substrate and gaseous environment, flow of carrier gas, distance between nozzle and substrate, droplet radius, solution concentration and solution flow [29-31]. It is an attractive deposition method for large surface film coatings and a wide range of metal oxide stoichiometries [32]. The apparatus comprises an atomizer, a substrate heater, a reaction chamber, a diffusion

tube, a temperature sensor (thermocouple), a carrier gas cylinder and pressure gauges [33, 34] as shown in figure 2.1 below.

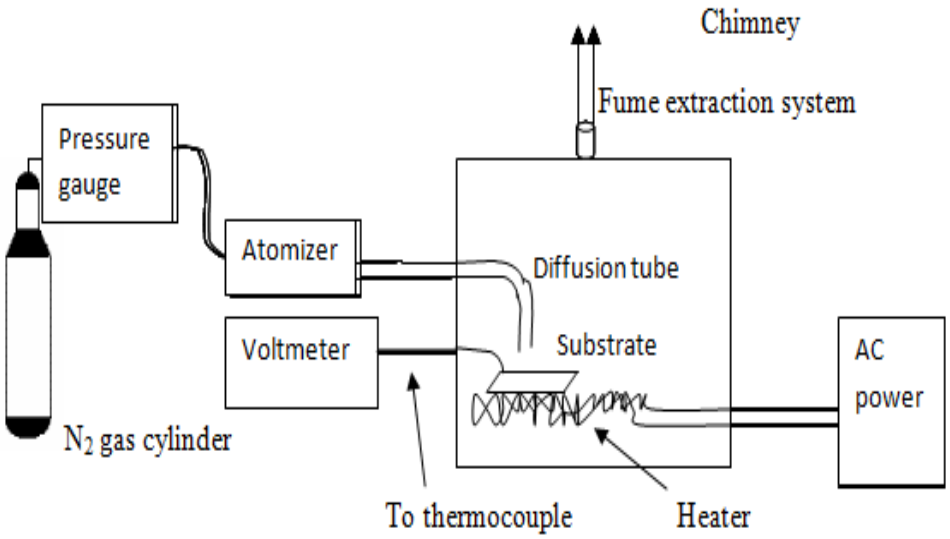

Figure 2.1 Schematic diagram of the modified spray pyrolysis unit.

The most important parameter in this technique of film formation is the substrate surface temperature. At higher substrate temperatures, the films become rougher and exhibit a more porous microstructure. If the temperature is too low, the films crack. The deposition temperature also influences the crystal formation, the texture and other physical properties of the deposited film. The precursor solution is the other important spray parameter, which affects the morphology and the properties of the deposited films. In addition, various additives in the precursor solution influence the film morphology and properties [35].

2.2 BASIC THIN FILM PROPERTIES

2.2.1 REFLECTANCE AND TRANSMITTANCE SPECTROSCOPY

The discussion of thin film optical properties begins with the basic idea of electromagnetic radiation incident from one medium to another. Figure 2.2 gives a single layer interface for light incident at angle θ_i to the normal. There is both reflection and refraction of the incident beam of radiation. Both the laws of reflection and refraction are satisfied. The angle of incidence θ_i has the same magnitude as the angle of reflection θ_r.

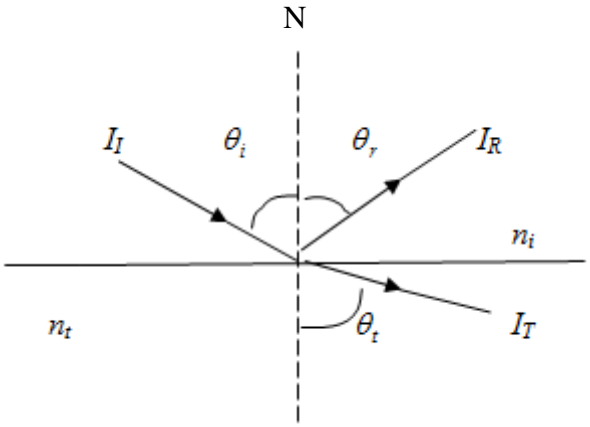

Figure 2.2 Beam of light incident at a single layer interface.

We have considered the intensity of the incident beam to be I_I, that of the reflected intensity to be I_R and that of the transmitted intensity to be I_T. Given that the refractive index of the first medium is n_i and that of the second is n_t, Snell's law gives

$$n_i \sin\theta_i = n_t \sin\theta_t . \qquad (2.0)$$

Taking the speed of light in medium one and medium two as v_1 and v_2 respectively, the ratio of the sine functions is equal to the ratio of the velocities in the two media as given by the relation

$$n = \frac{v_1}{v_2} = \frac{\sin\theta_i}{\sin\theta_t} \tag{2.1}$$

The relation in equation (2.1) is called the refractive index (n) of a medium. It must also be noted here that a beam of light impinging on a film-medium interface will undergo partial reflection and transmission. The transmitted component may consequently be partially or fully absorbed by the medium through which it moves.

The equations for the determination of the various optical parameters such as transmittance, reflectance and absorption amplitudes for air and multiple interface media are derived from considerations of Maxwell's and Fresnel's equations. The Maxwell equations are the set of four fundamental equations governing the behavior of electric and magnetic fields, whereas the Fresnel equations give the relations for the reflected and transmitted field amplitudes. Simplified forms of the Fresnel equations for the perpendicular and tangential electromagnetic components are [36]

$$\left(\frac{E_{or}}{E_{oi}}\right)_{\perp} = r_{\perp} = \frac{n_i\cos\theta_i - n_t\cos\theta_t}{n_i\cos\theta_i + n_t\cos\theta_t} \tag{2.2}$$

$$\left(\frac{E_{ot}}{E_{oi}}\right)_{\perp} = t_{\perp} = \frac{2n_i\cos\theta_i}{n_i\cos\theta_i + n_t\cos\theta_t} \tag{2.3}$$

Where E_{oi} is the electromagnetic field, E_{or} is the reflected electromagnetic field and E_{ot} is the transmitted electromagnetic filed.

$$\left(\frac{E_{or}}{E_{oi}}\right)_{II} = r_{\parallel} = \frac{n_t \cos\theta_t - n_i \cos\theta_i}{n_i \cos\theta_t + n_t \cos\theta_i} \tag{2.4}$$

$$\left(\frac{E_{ot}}{E_{oi}}\right)_{\perp} = t_{\parallel} = \frac{2n_i \cos\theta_i}{n_i \cos\theta_t + n_t \cos\theta_i} \tag{2.5}$$

where $r_{\perp}$, r_{II} are the reflection amplitude coefficients and $t_{\perp}$, t_{II} are the transmission amplitude coefficients for perpendicular and tangential components respectively when both media forming the interface are dielectrics.

When the electromagnetic fields are normal to the interface, we obtain the limiting case in which the cosine functions reduce to 1 and the amplitude coefficients can be written as follows:

$$\left(\frac{E_{or}}{E_{oi}}\right)_{\perp} = r_{\perp} = \frac{n_i - n_t}{n_i + n_t} \tag{2.6}$$

$$\left(\frac{E_{ot}}{E_{oi}}\right)_{\perp} = t_{\perp} = \frac{2n_i}{n_i + n_t} \tag{2.7}$$

$$\left(\frac{E_{or}}{E_{oi}}\right)_{\parallel} = r_{\parallel} = \frac{n_t - n_i}{n_i + n_t} \tag{2.8}$$

$$\left(\frac{E_{ot}}{E_{oi}}\right)_{\|} = t_{\|} = \frac{2n_i}{n_i + n_t} \tag{2.9}$$

The general reflectance *R* and transmittance *T* of an incident radiation flux at an angle θ_i on a surface are given by [36]

$$R = \frac{I_r \cos\theta_r}{I_i \cos\theta_i} \tag{2.10}$$

$$T = \frac{I_t \cos\theta_t}{I_i \cos\theta_i} \tag{2.11}$$

where I_i and I_r are the incident and reflected flux densities. As we can see, this is not a function of the surface area depends on the angular directions of the flux density.

For an air-single medium interface, we obtain

$$R = \left(\frac{n_i - n_t}{n_i + n_t}\right)^2 \tag{2.12}$$

$$T \cong \frac{4n_i n_t}{(n_i + n)^2} \tag{2.13}$$

For multiple reflections and transmissions the total transmittance and reflectance are obtained as summations of the individual amplitudes and are represented as [37]

$$T = \frac{r_1^{\,2} + 2r_1 r_2 \cos 2\delta_1 + r_2^{\,2}}{r_1^{\,2} + 2r_1 r_2 \cos 2\delta_1 + r_1^{\,2} r_2^{\,2}} \tag{2.14}$$

$$R = \frac{n_2 t_1^{\,2} t_2^{\,2}}{n_i\left(2r_1 r_2 \cos\delta_1 + r_1^{\,2} r_2^{\,2}\right)} \tag{2.15}$$

Here $\delta_1 = 2\pi\nu n_1 d_1 \cos\theta_1$ is the phase difference between successive radiation beams and ν is the wave number. For a material with extinction coefficient k we can define a complex refractive index N represented by

$$N = n - ik \tag{2.16}$$

At normal incidence, the reflectance is obtained from the relation

$$R = \frac{(n-1)^2 + k^2}{(n+1)^2 + k^2} \tag{2.17}$$

If $k = 0$, the relation (2.19) reduces to

$$R = \frac{(n-1\ )^2}{(n+1)^2} \tag{2.18}$$

for an air-substrate interface.

The Cauchy approximation given in equation 2.19 can be used to determine the wavelength dependent refractive index. This is [38]

$$n_\lambda = a + \frac{b}{\lambda^2} + \frac{c}{\lambda^4} \tag{2.19}$$

where a ,b, and c are constants that can be evaluated from at least three different wavelength values.

In experimental determination of the transmittance T, the reflectance R and the absorptance A, the following relations are used:

$$T = \frac{I_T}{I_O} \text{ x } 100\ \% \tag{2.20}$$

$$R = \frac{I_R}{I_O} \text{ x } 100\ \% \tag{2.21}$$

$$A = \frac{I_A}{I_O} \text{ x } 100\ \% \tag{2.22}$$

2.2.2 FILM THICKNESS DETERMINATION TECHNIQUES

There are many different ways in which the thickness of a thin film coating can be determined. As we have already seen, the thickness of a film is one of the most important parameters that affect its other properties and it has great bearing on how such a product can be used. We present the most applicable and convenient profilometry technique used in thickness determination for thin films coated on glass substrate.

Consider a coating on a transparent substrate such as glass. When light impinges on the surface of the film through to the substrate, it experiences double reflection. The first

reflection occurs at the air-film interface and the second one at the film-substrate interface. This leads to either constructive or destructive interference of the reflected amplitudes depending on their phase relationships. The phase relationship is normally determined by the difference in the optical path length of both these reflections. Fringes are observed in the selected wavelength region. These interference fringes resulting from specular reflectance are then used to determine the thickness *d* according to the relation [39]

$$d = \frac{m}{2D_n\sqrt{n^2 - \sin^2\theta}} \tag{2.23}$$

where *m* represents the number of interference fringes in the selected wavelength region, *n* is the effective refractive index of the composite, D_n is the wave number and θ the angle of incidence.

On the other hand, one can obtain the absorptance α_λ of the film from reflectance and transmittance measurements using the already determined film thickness [23, 40] for which the relation below holds when both reflectance and transmittance are not negligible. Thus [41]

$$\alpha_\lambda = \frac{1}{d}\ln\left(\frac{1-R_\lambda}{T_\lambda}\right) \tag{2.24}$$

If the reflectance is negligible, equation (2.26) can be approximated to

$$\alpha_\lambda = \frac{1}{d}\ln\left(\frac{1}{T_\lambda}\right) \tag{2.25}$$

2.2.3 STYLUS METHOD PROFILOMETRY

This method involves measurement of the mechanical movement of a diamond needle stylus having a tip radius of the order of 10^{-6} m. The profiling is done in the region of the thin film that forms a vertical step onto the substrate i.e., the edge of the thin film. The vertical movement of the stylus is computer-controlled and gives digital data of the profiled region. These data are plotted. The vertical difference between the highest and lowest values gives the height of the film step. This method is not suitable for soft thin films because the stylus tended to penetrate and scratch the film [37].

2.3 ELECTRICAL PROPERTIES

Accurate measurement of the electrical properties of thin films that are earmarked for applications in photovoltaic or thin film solar cells is cardinal. The dc electrical resistance depends to a large extent on the thickness and surface area of the coating. It also depends on the resistivity of the material used. We thus use the basic relation

$$R = \rho\frac{l}{A} = \rho\frac{l}{wd} \tag{2.26}$$

where w is the width of the coating and ρ is the material's resistivity. To obtain the resistivity, the measurement is normally done using the four-point resistance square

probe commonly referred to as the R_{square} probe. The resistance per square metre is is denoted by R_{square} and is given by [41]

$$R_{square} = \frac{\rho}{d} \tag{2.27}$$

The four-point resistance probe is used to measure film sheet resistance from which the resistivity is obtained. It comprises four equally-spaced tungsten metal tips with finite radius. The four tips are supported by a spring on a mechanical stage that moves up and down when measurements are being taken. The resistance is calculated from the voltage-current (I-V) characteristic measurements.

For a thin sheet between positions x_1 and x_2 shown in figure 2.3, the area of the circular section is $A = 2\pi xd$, where d is the film thickness.

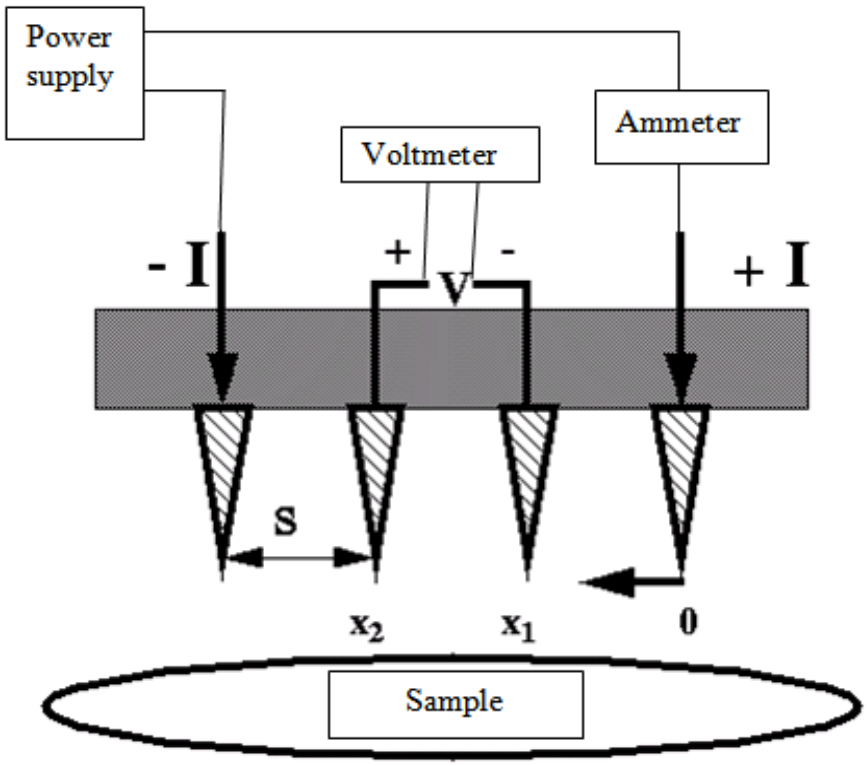

Figure 2.3 Basic connections of the four-point resistance probe.

It follows that the sheet resistance is the integral of the resistance of a small section *dx*, giving [42]

$$R = \int_{x_1}^{x_2} \rho \frac{dx}{2\pi x d} = \int_{s}^{2s} \rho \frac{dx}{2\pi x d} \tag{2.28}$$

where s is the separation distance of the metal tips, and x_1 and x_2 are points on the sample between which resistance was measured.

$$R = \frac{V}{2I} = \frac{\rho}{2\pi d} \ln 2 . \tag{2.29}$$

The current I is considered to flow in rings as opposed to spheres in the case of a thick film. The resistivity is obtained from [42,43]

$$\rho = \frac{\pi d}{\ln 2}\left(\frac{V}{I}\right) \tag{2.30}$$

where V is the voltage applied to the terminals of the probe.

2.4 EFFECTIVE MEDIUM THEORIES

Effective medium theories (EMT's) have been used to model and compare measured optical properties of composite media with the theoretically computed values. They are used as tools or mathematical models for evaluating the properties of the composite or doped material using the known properties of the constituent elements of the composite. Some materials are made up of the same type of atoms or molecules while other materials may be mixtures of two or more types of atoms or molecules. In some mixtures, the component material particles (atoms/molecules) retain their original properties. Such materials are called inhomogeneous mixtures. In other mixtures, the component materials lose their original identity and never retain their original properties but instead behave as a single new material with new properties. These materials are called homogeneous mixtures. Homogeneous mixtures are here referred to as effective media. An effective medium is considered to be that in which random unit cells or component particles of the inhomogeneous material are embedded such that the size of the particles and the spacing between them is much smaller than the wavelength of the incident electromagnetic radiation used in the analysis of the effective properties of the thin films [44-50]. A unit cell is the smallest unit of the crystal lattice that repeats itself

to form the crystal of the solid thin film. Thus effective medium models have been obtained using concepts of random unit cells which are sometimes referred to as inclusions. The effective medium treatment takes into account the fact that the resulting homogeneous medium is obtained by considering the overall effect of the presence of different inclusions (or random unit cells) in a heterogeneous material or composite. The inclusions referred to here are the particles of the film material and those of the doping substance. For example, a heterogeneous material would comprise ZnO particles and aluminium particles. When treated as an effective composite, the different particles present in the film material give an effective optical response which is expressed in terms of dielectric constants. This presents an effective behaviour of the film composite rather than that of the individual constituents or the host material itself. The properties of the composite are calculated from the known properties of its constituent particles.

Effective properties of thin film inhomogeneous composite media are modeled by different effective medium approximations that have been developed over a period of time and have undergone modifications to suit the specific cases of interest. The most common EMT used is the Maxwell-Garnet theory, which is essentially a modification of the Lorentz-Lorentz formula and is sometimes referred to as the Clausius-Mosotti relation. The others are the Bruggeman, Mie and Ping Sheng theories. The materials are treated in terms of effective relative dielectric functions or conductivities by considering properties of unit cells embedded in a material resulting into a composite inhomogeneous medium [51]. The known properties of the cells embedded in the host material are used in modeling the properties of the effective medium.

Assumptions about the aggregate structure of the medium under study are made to simplify the complexity of the problem and to allow the theory to suit the case being studied. The basic idea is to define an effective dielectric permeability ε of an effective medium which is assumed to result from an inhomogeneous composite material having different particles or inclusions with different dielectric permeability. Therefore, proposals about the possible microstructure of the materials are made. A proposal by Niklasson for a two-component mixture composed of random unit cells cited by Chibuye [52] is that such a mixture may exist in two phases: in the first phase the constituent particles of the different components remain separated while in the second phase, the constituent particles join together to form aggregates as in figure 2.4 [53].

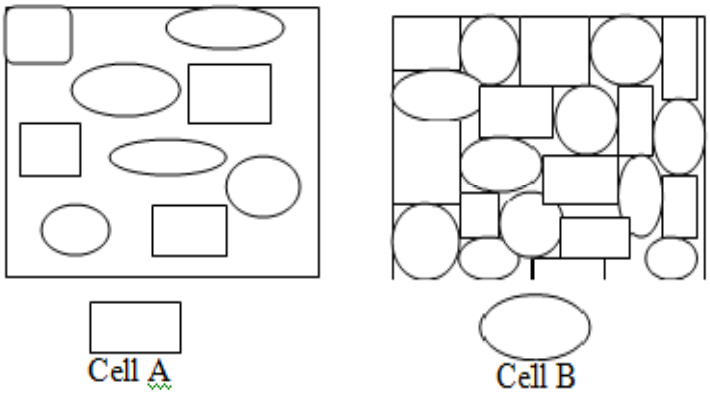

(a) Separated-grain structure (b) Aggregated-grain structure

Figure 2.4 Microstructure configurations of materials.

The optical properties of an inhomogeneous medium are described in terms of dielectric functions and magnetic permeabilities both of which may be complex and are frequency or wavelength dependent. Individual EMTs are concisely described and the

microstructure assumptions illustrated. The expected transition is one that derives an effective medium from an inhomogeneous one according to the following illustration in figure 2.5 [54].

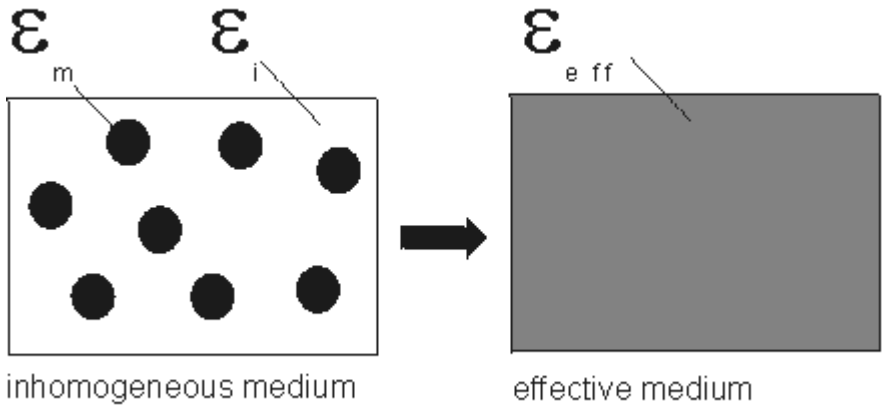

Figure 2.5 Illustration of medium conversion from inhomogeneous to effective medium.

2.4.1 MAXWELL-GARNETT EFFECTIVE MEDIUM THEORY

This theory was initially developed to model the effective permittivity of heterogeneous media consisting of single dispersed spheres arranged in a cubic lattice structure. A cubic lattice structure is one where the three crystal axes are at right angles to each other with equal repetitive intervals along the axes [55]. It considers random unit cells A and B imbedded in an effective medium having respective dielectric permeability ε_A and ε_B respectively as illustrated in figure 2.6.

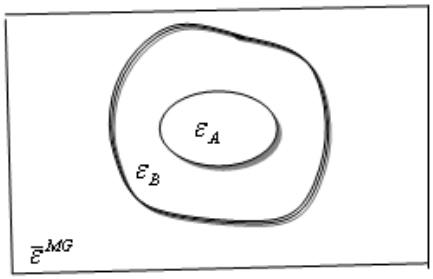

Figure 2.6 Maxwell-Garnett effective medium unit cell configuration.

The unit cells are considered to be small spheres with radii *a* and *b*. In this limit, the Maxwell-Garnett effective dielectric permeability is given by [4]

$$\bar{\varepsilon}^{MG} = \varepsilon_B \left(\frac{\varepsilon_A + 2\varepsilon_B + 2f_A(\varepsilon_A - \varepsilon_B)}{\varepsilon_A + 2\varepsilon_B - f_A(\varepsilon_A - \varepsilon_B)} \right) \tag{2.31}$$

where f_A is the volume fraction of the inclusions forming the effective medium and is given by

$$f_A = \frac{a^3}{b^3} \tag{2.32}$$

where a denotes the radius of the inner sphere and b that of the outer sphere. This treatment has been applied to a simplified problem where the medium composite is made of just two inclusions as in the case of the thin film coatings we have been considering in this work.

2.4.2 THE BRUGGEMAN THEORY

The Bruggeman approach differs from the Maxwell-Garnett approach by the arrangement of the composite microstructure and by the fact that no particular phase constituent of the composite is preferred. It assumes a structure that comprises random spherical unit cells embedded in an effective medium as in figure 2.7. In this treatment, both particle constituents are given equal treatment. One phase of the composite has a dielectric function ε_A while the other has a dielectric function ε_B and the result is a medium with an effective dielectric permeability $\bar{\varepsilon}^{Br}$ as illustrated in figure 2.7. Each unit cell has the probability f_A to have dielectric permeability ε_A and 1- f_A to have ε_B.

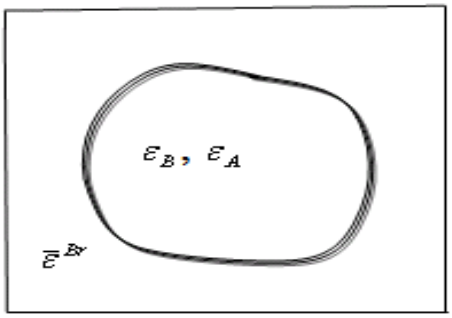

Figure 2.7 Bruggeman effective theory random unit cell configuration.

The equation for the effective Bruggeman dielectric permeability is obtained by solving [43*,56]

$$f_A\left(\frac{\varepsilon_A-\bar{\varepsilon}^{Br}}{\varepsilon_A+2\bar{\varepsilon}^{Br}}\right)+(1-f_A)\left(\frac{\varepsilon_B-\bar{\varepsilon}^{Br}}{\varepsilon_B+2\bar{\varepsilon}^{Br}}\right)=0 \qquad (2.33)$$

Solving the above equation, we obtain multiple values for $\bar{\varepsilon}^{Br}$. Not all the multiple values will have a physical meaning and thus the results must be interpreted to qualify the solutions.

2.4.3 THE MIE THEORY

The Mie theory was formulated in 1908 [59]. It is an analytical solution to Maxwell's vector equations for light scattering by an isotropic sphere which is considered to be a homogeneous medium upon which a magnetic wave is incident. It is sometimes referred to as the Lorentz-Mie theory or the Lorentz-Mie-Debye theory. The Mie theory assumes electromagnetic scattering by a spherical homogeneous particle in a medium. The relative refractive index is considered to be a ratio between the refractive index of the particle and that of the medium.

In application, this theory calculates the scattered electromagnetic waves at all field points in a spherical particle embedded in a medium. Here, the solution of the wave equation is given as [57, 58]

$$\begin{bmatrix} E_l^s \\ E_r^s \end{bmatrix} = \frac{\exp(-ikR + ikz)}{ikR} \begin{bmatrix} S_2 S_3 \\ S_4 S_1 \end{bmatrix} \begin{bmatrix} E_l^i \\ E_r^i \end{bmatrix} \tag{2.34}$$

where $k = \frac{2\pi}{\lambda}$, E_l^i, E_r^i are the parallel and perpendicular components of the incident electrical field whereas E_l^s and E_r^s are the parallel and perpendicular components of scattered electric field. The Mie theory solutions for scattering amplitudes are [58*]

$$S_1(\Theta) = \sum_{n=1}^{\infty} \frac{2n+1}{n(n+1)} \left[a_n \pi_n(\cos\Theta) + b_n \tau_n(\cos\Theta) \right] \tag{2.35}$$

$$S_2(\Theta) = \sum_{n=1}^{\infty} \frac{2n+1}{n(n+1)} \left[b_n \pi_n(\cos\Theta) + a_n \tau_n(\cos\Theta) \right] \tag{2.36}$$

where $\pi_n(\cos\Theta) = \frac{1}{\sin\Theta} P_n^l(\cos\Theta)$ and $\tau_n(\cos\Theta) = \frac{d}{d\Theta} P_n^l(\cos\Theta)$ are the Mie angular functions and the P_n^l are the associated Legendre polynomials.

2.5 STRUCTURE ANALYSIS

The surface structure of a coating is usually obtained by experimental determination. It is not feasible to predict the structure from general theory because film surface structure comes out in different ways depending on the procedure and conditions to which the process is subject. There exist a number of techniques by which the surface morphology and chemical composition of coated films are studied. These include but are not limited to X-ray diffraction (XRD), scanning or transmission electron microscopy, atomic force microscopy and optical microscopy [59]. The basic information that is obtained by these techniques during surface structure characterization is the crystal structure and orientation, film grain size, surface height profile and surface imaging.

The parameters of the surface are important in characterization techniques because they influence electrical and optical properties. A comparison between a rough and a smooth film of the same thickness reveals that the reflection on a rough surface is more diffuse than that on the smooth one where it is mostly specular. On the other hand, a rough

surface will have high sheet resistance because of the deformations that tend to reduce the effective electron path.

CHAPTER III

EXPERIMENTAL TECHNIQUES

3.1 SAMPLE PREPARATIONS

Sample preparation involved two stages; preparation of substrates and precursor solutions and preparation of the film sample itself. Further, explanation is given of the various measurement systems used in this work.

3.1.1 SUBSTRATE PREPARATON

Standard microscope glass slides were cleaned using a detergent liquid and then washed in toluene and rinsed with distilled water. They were then dried using compressed air and left in a clean place on soft laboratory tissue in readiness for use. The detergent's effect was to remove any dirt that may have accumulated on the slides while the toluene removed any oily layers on the substrate. The purpose of the distilled water was to wash away the toluene.

3.1.2 PREPARATON OF ZnO PRECURSOR SOLUTION

In the preparation of the precursor solution for growing ZnO we used zinc chloride ($ZnCl_2$) as the raw material. The $ZnCl_2$ was weighed on an electronic balance which reads to an accuracy of 0.1 mg. This was doped with aluminium by weighing and adding aluminium chloride hexahydrate ($AlCl_3.6H_2O$) to the $ZnCl_2$. The mixture was then placed in a flat bottomed flask. This was then dissolved in distilled water with the addition of a little hydrochloric acid (HCl) which acted as a complexing agent,

preventing precipitation and thus making the solution stable. Different spray solutions of different mass concentrations and doping levels were prepared.

3.1.3 PREPARATON OF Al_2O_3 PRECURSOR SOLUTION

In a similar manner, aluminium chloride hexahydrate ($AlCl_3.6H_2O$) was weighed and placed in a flat-bottomed flask. A doping amount of $ZnCl_2$ was also measured and added to the flask. Distilled water and a little hydrochloric acid were added and the flask shaken well for the mixture to dissolve. Solutions with varying doping amounts were prepared. The variation of doping was to help optimize the properties of the films to be grown from these solutions.

3.1.4 TEMPERATURE CALIBRATON OF THE SPRAY PYROLYSIS OVEN

The spray pyrolysis oven temperature was monitored by a nickel-chromium thermocouple. This thermocouple was calibrated against the temperature-graduated Carbolite oven stationed in the Solid State Physics Laboratory of the Physics Department at the University of Zambia. The thermocouple was connected to a voltmeter that served as the output device for the measurement of the electromotive force (EMF) produced due to the temperature difference on the nickel-chromium wire junctions of the thermocouple. The oven was set for temperatures ranging from 100^{o}C to 700^{o}C in steps of 50 and for each temperature the corresponding EMF generated by the thermocouple was noted. A calibration plot of EMF against temperature was made. During film growth, the EMF read from the voltmeter was compared with the calibration curve to obtain the corresponding spray temperature. The principle behind the operation

of the thermocouple is that the generated EMF is directly proportional to the temperature difference across the thermocouple junctions.

The oven temperature was measured as a function of time and plots of temperature versus voltage and temperature versus time were made. This helped to heat the oven to the required temperature by just considering the time for which it was on. This was always verified by actual temperature measurement according to the calibration.

The spray pyrolysis oven which had earlier been constructed in the lab was modified by partially dismantling it. The aluminium walls of the heating chamber were replaced by asbestos and the roof top was improvised so as to minimize heat losses through the fume extraction vent. The top part of the oven had some wood mounted on it. When high temperatures were reached, the wood would slowly start to burn. To avoid this occurrence, the wood was removed and as before replaced by aluminium sheets. With this in place, reasonable temperature values could be achieved easily. Figure 3.1 shows the initial appearance of the heating chamber.

Figure 3.1. Basic appearance of the heating chamber (oven) showing the side walls and the base built from asbestos material.

A set of four heating elements, with power a rating of 850W, was placed at the base of the chamber in a parallel wiring configuration to give maximum power output. This configuration was able to raise the temperature in the oven up to 500^{o}C after 2 hrs of heating. In the process of film growth, two heating elements blew up and could not be replaced as they were not locally available. With the two remaining elements, temperatures up to 350^{o}C could be reached in about 250 minutes of heating. Oven and substrate temperatures were monitored using a calibrated nickel-chromium thermocouple.

Other components of the spray pyrolysis unit comprised a nitrogen gas cylinder, connecting tubes, a set of pressures gauges and an atomizer connected to the diffusion

tube running into the heating chamber where the substrate was placed. The other end of the atomizer was connected to the gas cylinder through a set of three precision pressure gauges. Since the fumes resulting from the spray pyrolysis processes could be a health hazard, a fume extraction pipe was extended to the roof top of the building housing the laboratory so that all the gases were expelled from the building. This was aided by an extraction fan.

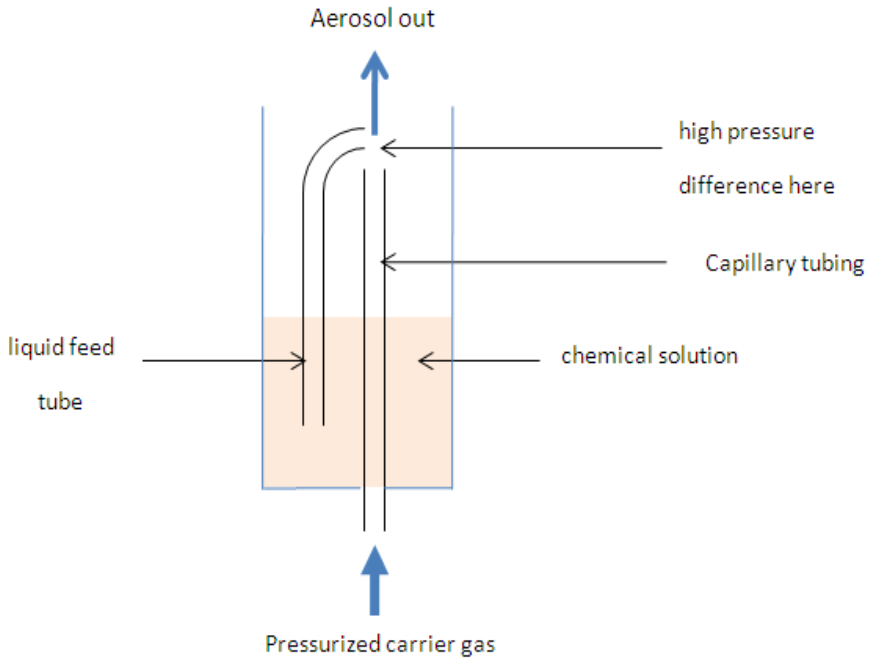

Figure 3.2 Schematic diagram of the spray pyrolysis atomizer or nebulizer.

Figure 3.3 Physical assembly of the spray pyrolysis unit.

3.1.5 GROWTH OF ZnO AND Al_2O_3 THIN FILMS

In the process of growing thin films, a solution of ZnO or Al_2O_3 was placed in the atomizer as shown in figure 3.2. A substrate was placed in the heating chamber and allowed to heat to the required temperature before spraying was done. When a desired temperature was reached, as monitored by a calibrated thermocouple on a voltmeter, spraying was done for a specified time and at an appropriate carrier gas pressure monitored on the multi-stage pressure regulator. The carrier gas used was nitrogen. The respective solutions were sprayed through an atomizer or nebulizer onto standard microscope glass substrates to form solid thin films.

The spray pyrolysis mechanism is such that when the knob of the gas cylinder is opened, the gas comes out with high pressure and enters the capillary tubing of the atomizer. At the ends of the capillary tubing and the liquid feed tube, a high pressure difference is created between the ends of the liquid feed tube which causes the precursor solution to come out and the aerosol is transported to the substrate via the diffusion tube. The solution lands on the hot substrate where it solidifies and forms a thin film. Different films were obtained for different spray parameters. Optimization of film properties was achieved by varying substrate temperature, solution concentration, carrier gas pressure, variation of doping levels, spray time and multiple coating of films. The samples were labeled for easy identification.

The process flow chart below explains the stages of thin film coating from the first step to the last, including repeated tasks. The flow chart provides two loop options: one for a repeated process with the same precursor solution and the other where a new precursor solution had to be prepared and the process started over again. YES in the flow chart meant that the same chemical solution was to be used. For this option, the process repeating point was heating a substrate. On the other hand, NO, as shown on the chart, meant that a new solution had to be prepared, which meant starting the process again at the step of weighing the sample materials.

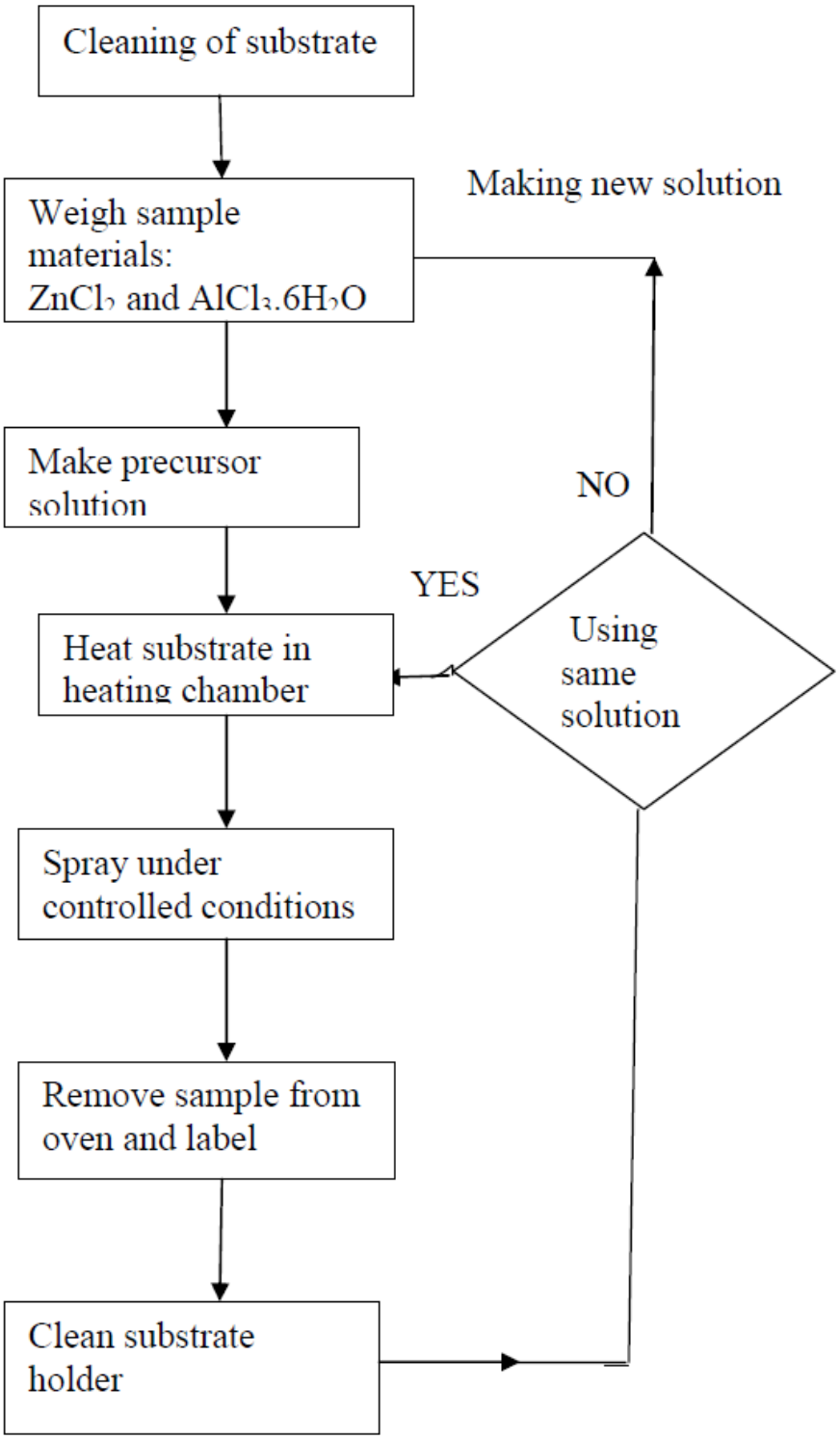

Figure 3.4 Experimental procedure flow chart.

After each growth process, the sample holder was cleaned to reduce contamination of the next sample. The grown samples were kept in a desiccator to maintain their form and avoid possible contamination and interference from the environment until after the various measurements were done. The flow chart in figure 3.4 gives the experimental procedure for the growth of the spectrally selective thin films of both zinc and aluminium oxides.

3.2 TRANSMITTANCE AND REFLECTANCE MEASUREMENT SYSTEMS

Figure 3.5 shows a setup of the system for measuring the reflectance and transmittance of the film samples. It comprises the spectrophotometer and computer which are interfaced. Characterization in the VIS-NIR wavelength range was performed using the Lambda 19 spectrophotometer located in the Solid State Physics laboratory at the University of Zambia. Its operating procedure requires that the computer is switched on first and switched off last. The spectrophotometer has an integrating sphere and two lamps, one for the UV and the other for VIS-NIR spectral regions respectively. Before taking optical measurements of the samples, background correction was performed. For transmittance measurements, the sample was mounted on one side of the integrating sphere's inlet hole facing the source of the incident beam of electromagnetic radiation. With the help of the software, the ratio of the transmitted amplitude to the incident one was recorded as a percentage value for each wavelength in the assigned wavelength spectral range. The results were imported to Sigma Plot 8.0 software for analysis. On the other hand, reflectance measurements were made by placing the sample on the exit hole of the integrating sphere so that the coated side was facing the incident beam of

electromagnetic waves. Then a beam of electromagnetic waves (EM) was allowed to impinge on the sample. The spectrophotometer recorded the reflected fraction of the incident beam. This was again imported to Sigma Plot 8.0 for analysis.

Figure 3.5 Perkin Elmer Spectrum BX FT-IR system at the University of Dar es Salaam Solar Energy Research Laboratory.

The setup in figure 3.5 was used for transmittance and reflectance measurements in the far infrared region. This particular one is the Perkin Elmer Spectrum BX FT-IR system located at the Solar Energy Research laboratory at the University of Dar es Salaam. The configuration of this spectrophotometer requires that the spectrophotometer is switched

on before the computer is switched on and that the computer is off before it is switched on. In fact this machine was always on so that only the computer was turned on and off each time the system was used. Transmittance measurements with this system were done in a manner similar to the case of the Lambda 19 spectrophotometer. Figure 3.6 shows a picture of the integrating sphere and the positions where samples were placed during transmittance and reflectance measurements.

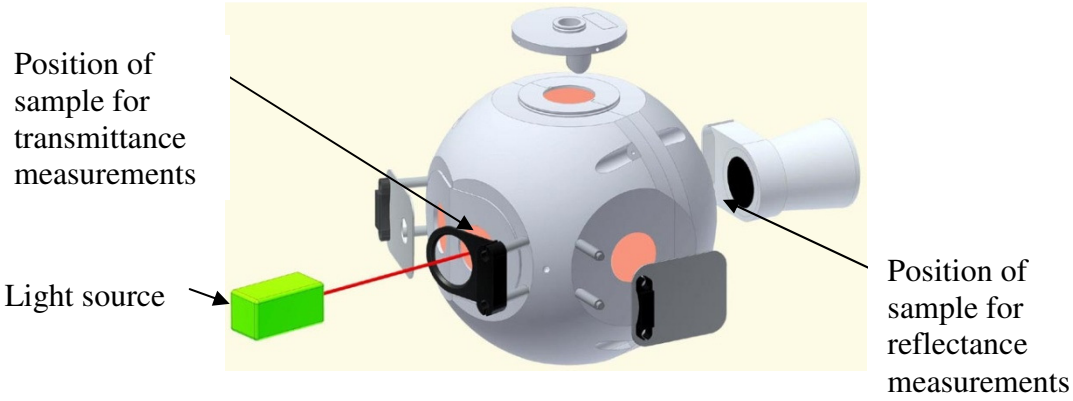

Figure 3.6 Integrating sphere for a spectrophotometer [60].

Reflectance measurements were performed with the help of a silvered glass mirror standard. Firstly, the silvered glass mirror was placed in the sample holder and the reflectance taken. The mirror was then replaced with the sample and again the reflectance measurements taken. In the case of IR reflectance, the values obtained are ratios of sample reflection amplitudes to that of the standard. The standard used was 96 per cent reflecting. To correct for this, the reflectance result was multiplied by 0.96. The measurement procedure was the same for all ZnO and Al_2O_3 samples.

3.3 THICKNESS MEASUREMENT SYSTEM

The thicknesses of the samples were obtained using the Tencor Alpha Step profiler interfaced with a computer as shown in the schematic diagram in figure 3.7. The films were coated at the centre of the substrate so that the edges of the film and the surface of the substrate formed a step. Then the stylus of the alpha step was positioned on the surface of the coating. Readings were taken as the stylus moved over the surface of the coating and as it descended onto the substrate. The differences between the minimum and the maximum readings were taken as the thickness of the thin film '*d* '. Figure 3.8 gives the schematic diagram of the thickness profiling.

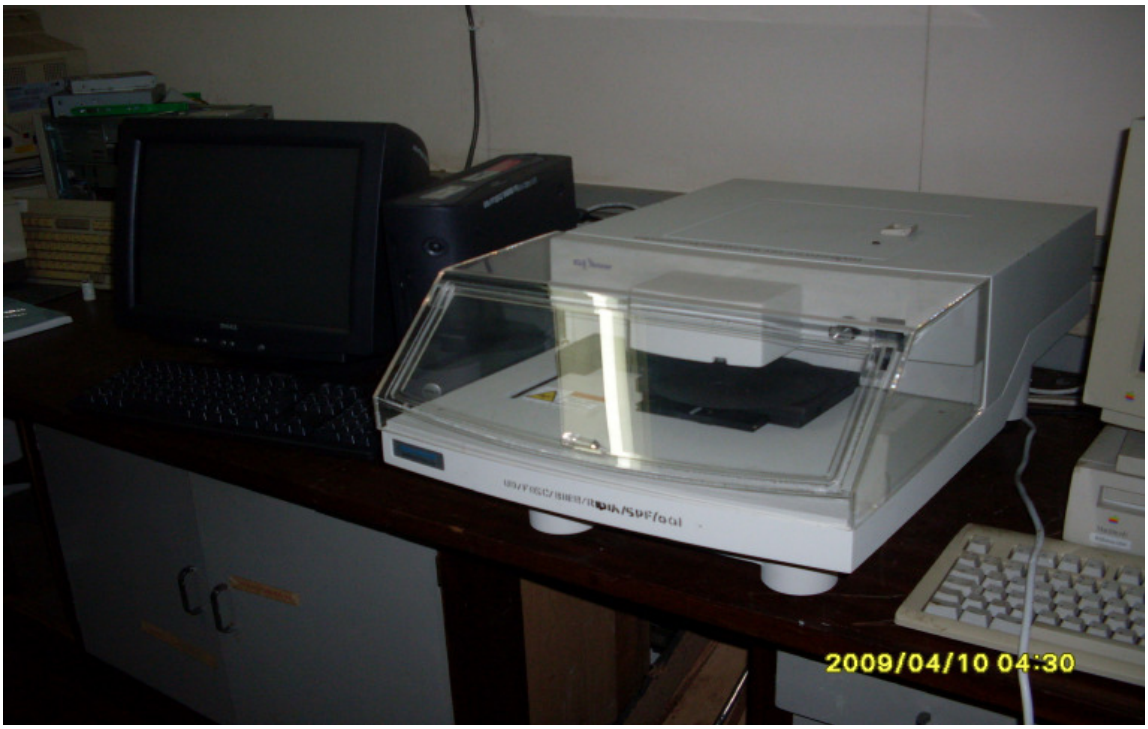

Figure 3.7 Tencor Alpha Step profiler.

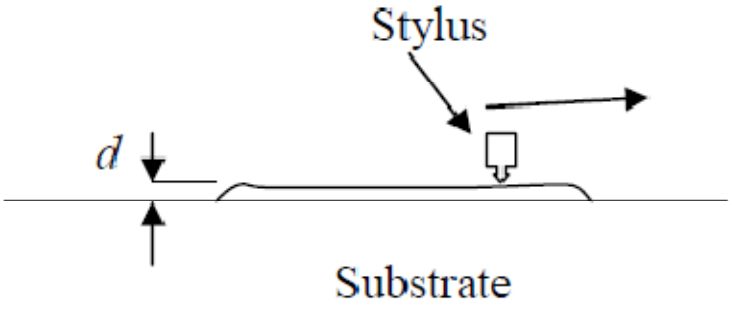

Figure 3.8 Schematic diagram of thickness profiling.

3.4 ATOMIC FORCE MICROSCOPE (AFM)

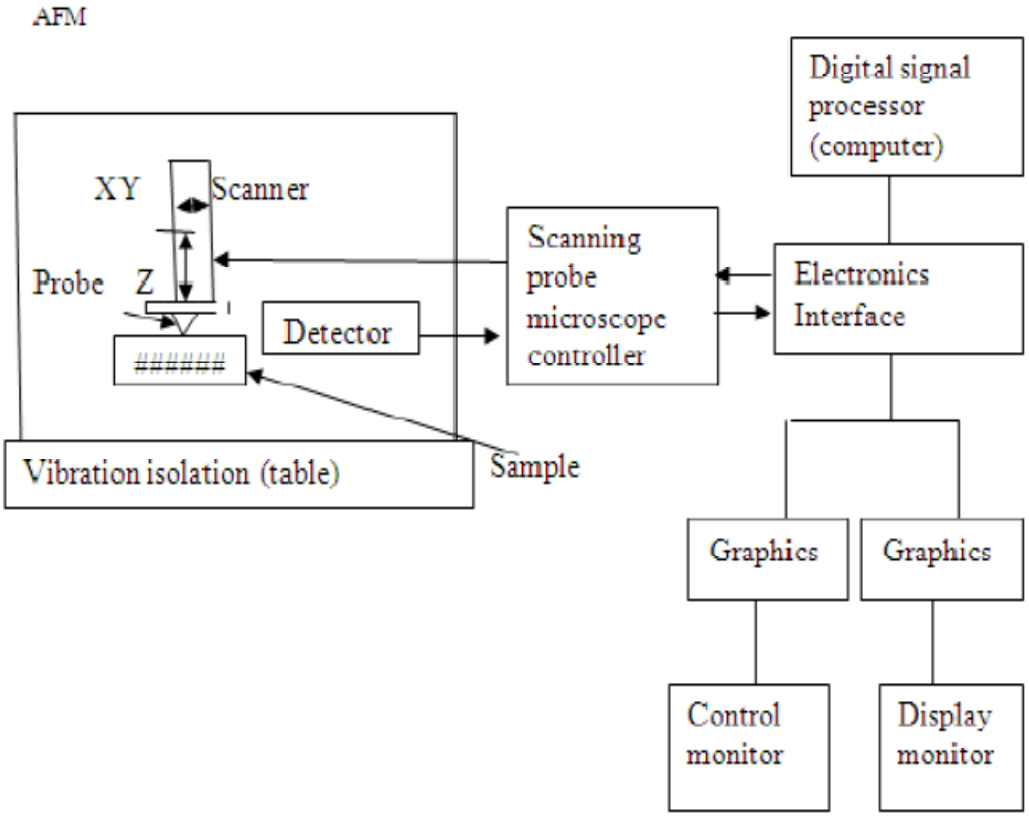

Figure 3.9 Basic components of the atomic force microscope.

Figure 3.10 System components of the AFM: electronics interface, microscope, objective lens, Optical lighter, control monitor, display monitor and CPU.

Figure 3.10 shows the physical setup of the atomic force scanning system with the other accessories included. The schematic diagram of the same system is given in figure 3.9 [61]. It shows the basic components of the AFM, also called a scanning probe microscope (SPM). The AFM was placed on a vibration isolation table so that the scanning process was not affected by background vibrations. The sample was placed in the sample holder following a step by step procedure as described in the SPM training note book. The objective lens was used for proper positioning of the cantilever over the sample and fixing the laser beam on the probe while the lighting was provided by the optical lamp system. The scan was controlled using the control monitor while observing

the output on the display monitor. The embedded software was used for analyses that included section roughness, particle size and surface plots. The AFM was operated in tapping mode which had been set as the default mode. Tapping mode AFM operates by scanning a tip attached to the end of an oscillating cantilever. The cantilever tip lightly taps on the sample surface during scanning thus contacting the sample surface at the end of its swing. The tapping mode produces higher lateral resolution and does not scratch the sample. The AFM can alternatively be operated in contact mode.

3.5 THE FOUR POINT RESISTANCE PROBE

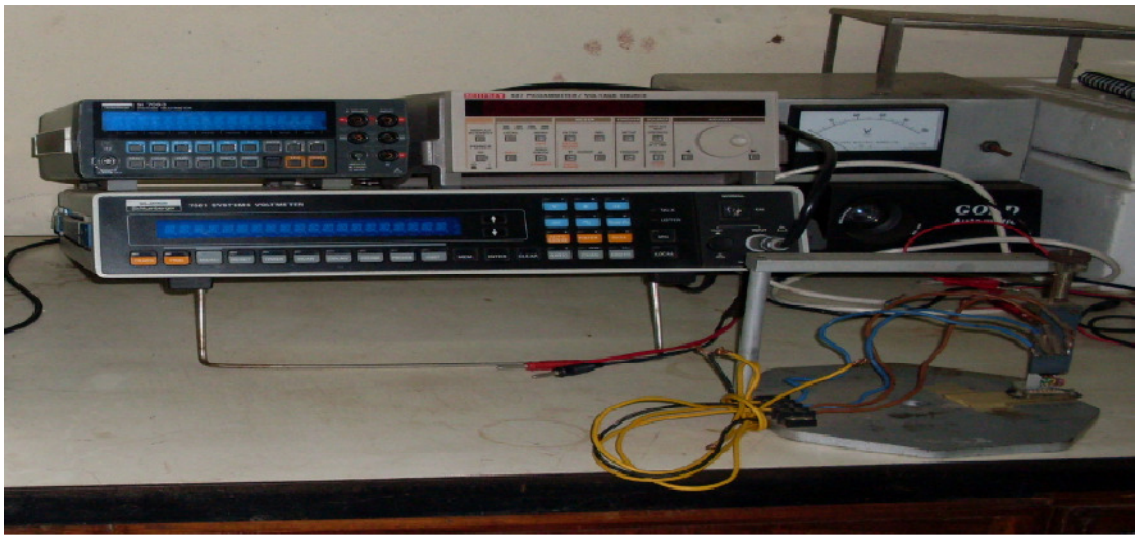

Figure 3.11 Physical arrangement of the four point resistance probe.

Measurement of film sheet resistance was indirectly done using the four-point square probe. Characteristic I-V values were measured and the resistance and film resistivity calculated from the relations (2.31) and (2.32) given in chapter two. The sample was placed on the sample stage and pressed by the four tips of the probe by lowering the

mechanical stage. Direct current was then supplied to the outer tips and the potential difference between a section of the film, x_1 and x_2 was read off from the voltmeter connected in parallel with this section. At least three readings were taken for each sample and the mean of the calculated resistance recorded as the sheet resistance for that sample.

CHAPTER IV

RESULTS

Results for the temperature calibration curve of the spray pyrolysis coating unit as a function of time, transmittance, reflectance, absorptance, surface characteristics, film surface I-V characteristics and thickness measurements were obtained and these are presented in this chapter.

4.1 TEMPERATURE CALIBRATION

The data for the calibrated nickel-chromium thermocouple were used to obtain a temperature profile in the oven and for monitoring the substrate temperature during and after spraying. We see from the calibration curve that the voltage generated in the thermocouple is linearly proportional to the temperature. Therefore, by reading the thermocouple output voltage, we were able to translate it to temperature by means of the calibration curve shown in figure 4.1.

It was also important to know roughly when a required temperature of the substrate was reached after switching the system on. This was achieved by obtaining the oven temperature profile as a function of time. The temperature rise was sharp when the heating elements were just switched on and it stabilized slowly as the elapsed time approached 120 minutes.

Figure 4.1 shows the plot of the calibration curve for the nickel-chromium thermocouple obtained using the temperature-graduated Carbolite oven in the Solid State Physics Laboratory at the University of Zambia.

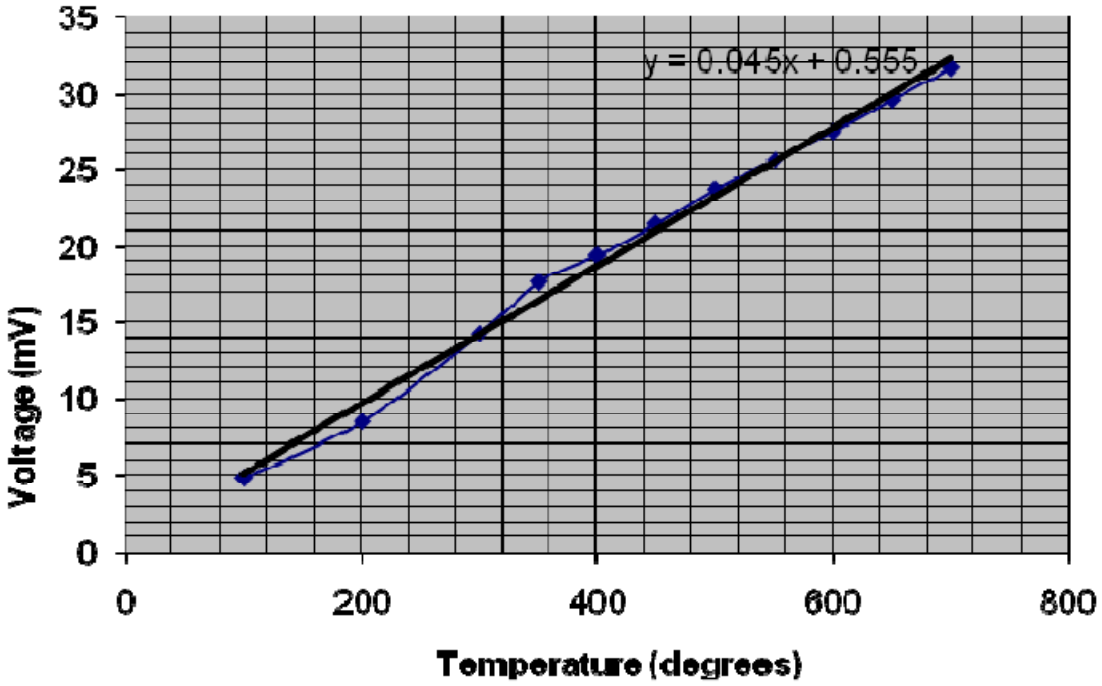

Figure 4.1 Thermocouple temperature calibration curve.

Figure 4.2 shows the temperature versus time profile for the oven. From this temperature profile, it is seen that we could reach temperatures of about 500^{o}C after about 120 minutes of heating when all the four heating elements were working and 300^{o}C when only two heating elements were in use. Two elements blew up after the oven was used for some time and we had to make do with only two elements as we could not find suitable elements for replacement.

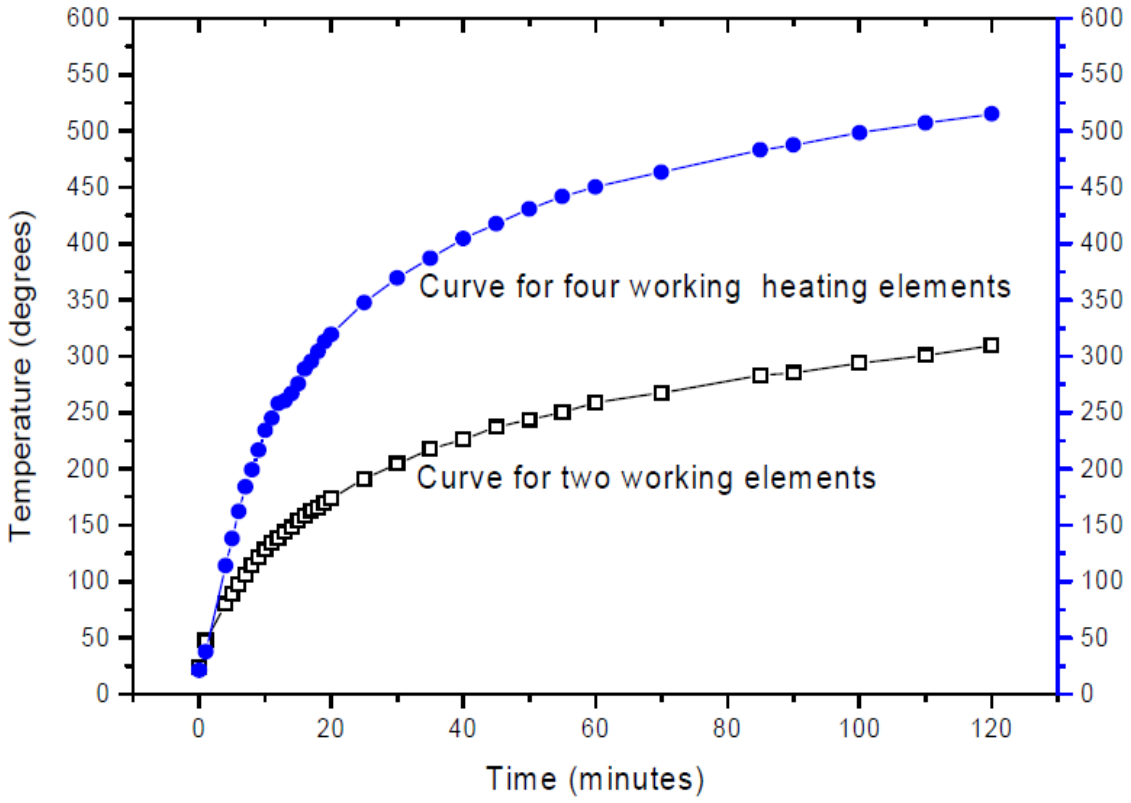

Figure 4.2 Oven temperature as a function of time.

4.2 FILM THICKNESS

The thickness of a thin film depends greatly on the growth parameters. Different thicknesses were obtained for films grown using different growth parameters such as spray time, pressure, concentration of precursor solution and substrate temperature. It was observed that more concentrated solutions gave thicker films as compared to less concentrated ones under the same conditions. This is expected because in the former case there are more solute molecules that result into solid film after spraying. The other key parameter that directly affected thickness was spray time. It was further observed that longer spray times resulted into thicker films as one would expect. The pressure at

which the film was sprayed gave an inverse relation to the thickness of the film. Higher spraying pressure resulted in films with lower thickness. Logically it would be expected that higher pressure should result into thicker films since more solution would be picked up. The reasons for the counter-intuitive results are as follows: at high pressure the picked up precursor solution is sprayed over a much larger area and sometimes even sent off the substrate surface as compared to the low pressure conditions. This results in the formation of thinner films. Higher spray pressure also resulted into rapid cooling of the substrate. This meant that spraying time had to be reduced so that the coating was done at nearly the same temperature. This again led to thinner films on the substrate.

Thickness values were obtained using the Tencor Alpha Step Profiler. The new and interesting result from films prepared by the spray pyrolysis method was that the edges of the thin film resulting from spray pyrolysis tended not to give a step ending but rather steadily reduces in height from the top to the surface of the substrate. Thus, thickness measurements using the step technique were performed to determine the height of the film by obtaining a film surface profile from the top surface to the bottom. The trend observed was that the height profile was a slanting curve punctuated by periodic dips suspected to be caused by the stylus' penetration into the film material and noise. The step graph for nearly all the samples had an appearance similar to the one in figure 4.3 and figure 4.4. We notice a steady slope from the top of the film to the base of the substrate. This implies that in the spray pyrolysis process, we obtained non-distinct film edges but rather a steady decrease in film thickness from its centre to the edge of the coated part of the substrate. It means that the film edges were not cleared marked to

show a step. Thicknesses ranging from 0.14 μm to 87.7 μm were achieved in this research. It has been noted that time of spray had the greatest influence on the thickness of the resulting coating film. The obtained thickness values of the samples are given in table 4.1.

The thickness of a given film has an impact on the efficiency of the solar cell made from such material. The thicker films have high absorption and low solar transmittance. From the samples presented in this work, those with low thickness are best suited for application as transparent conducting coatings. This is because they give high solar transmittance and this would improve the efficiency of the solar tandems by allowing more of the solar energy to get through which later converts to electric current through conduction in the solar tandem layers. Lower thicknesses of up to 0.14 μm have been achieved in the spray pyrolysis coating process. This result is important because we expect improved light harvesting when these coatings are used in the making of thin film solar cells [58].

We observe from figure 4.3 and figure 4.4 that the thickness profiles for ZnO and Al_2O_3 were different. This was attributed to the fact that their surface structures were not exactly the same. For double-layered coatings, the depressions in the thickness profile were minimized since the second coating layer leads to a smoother film surface.

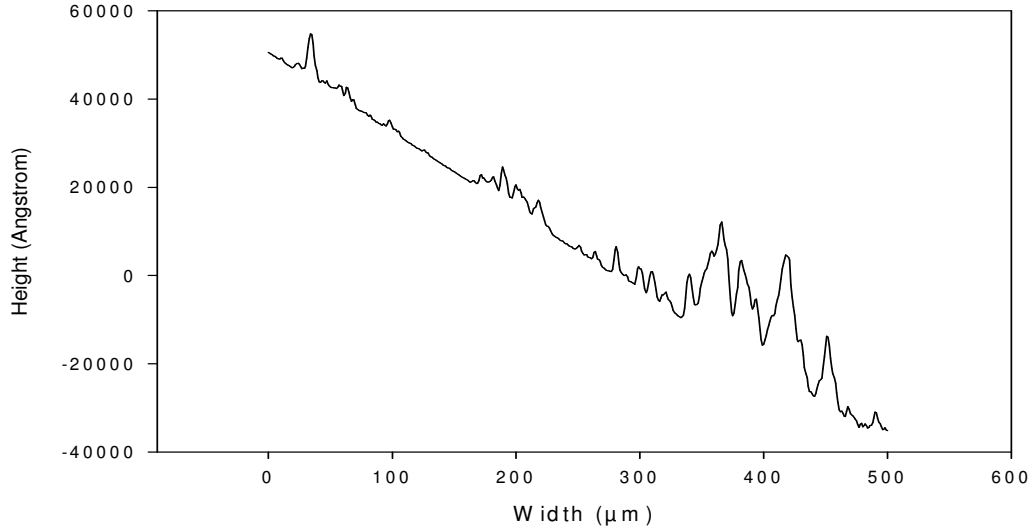

Figure 4.3 Thickness profile of double layer Al_2O_3 thin film

The thickness indicated in figure 4.3 is 8.2 μm and that in figure 4.4 is 6.2 μm.

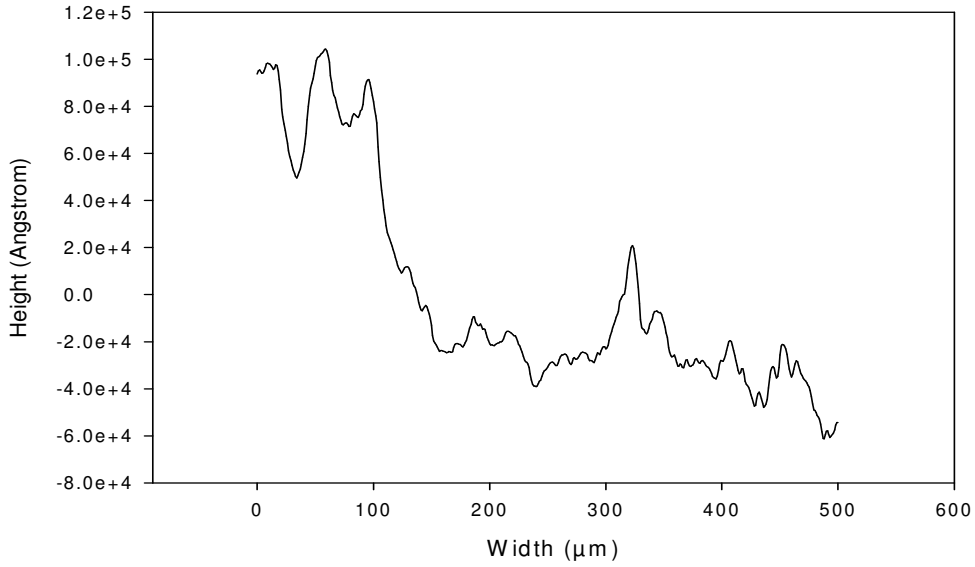

Figure 4.4 Thickness profile of single layer ZnO thin film.

4.3 TRANSMITTANCE MEASUREMENTS

As already stated in the previous chapter, the transmittance of the samples for the UV-VIS-NIR wavelength ranges were obtained using the Elmer Lambda 19 spectrometer in the Solid State Physics Laboratory at the University of Zambia. Characterization in the far infrared was done using the BX FT-IR system at the University of Dar es Salaam.

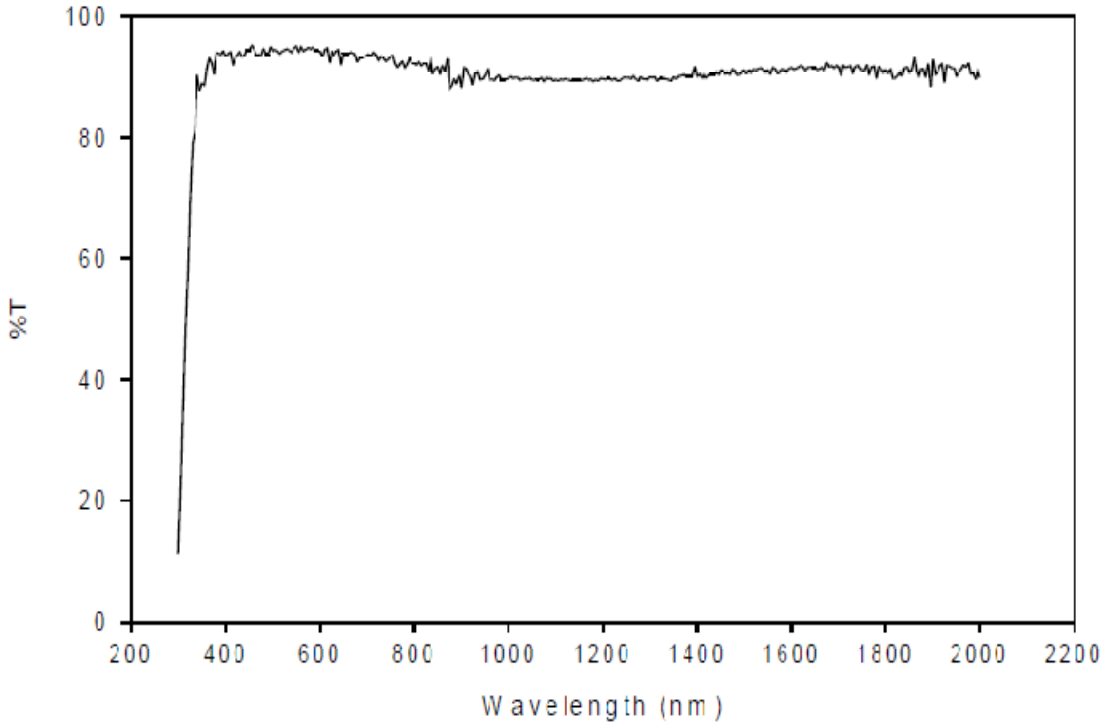

Figure 4.5 Transmittance curve for uncoated glass slide in UV-VIS-NIR region.

Figure 4.5 shows the transmittance characteristic of the uncoated glass substrate in the UV-VIS-NIR region. There is a transmittance cut-off of the UV light and a near 90 per cent transmission in the wavelength range 200-2500 nm. Figure 4.6 is a continuation of the transmission characteristic of the uncoated substrate in the infrared region. We

observed that the transmittance dropped to 60 per cent in the wavelength range 2500 nm to 4000 nm and steadily fell to zero in the far infrared.

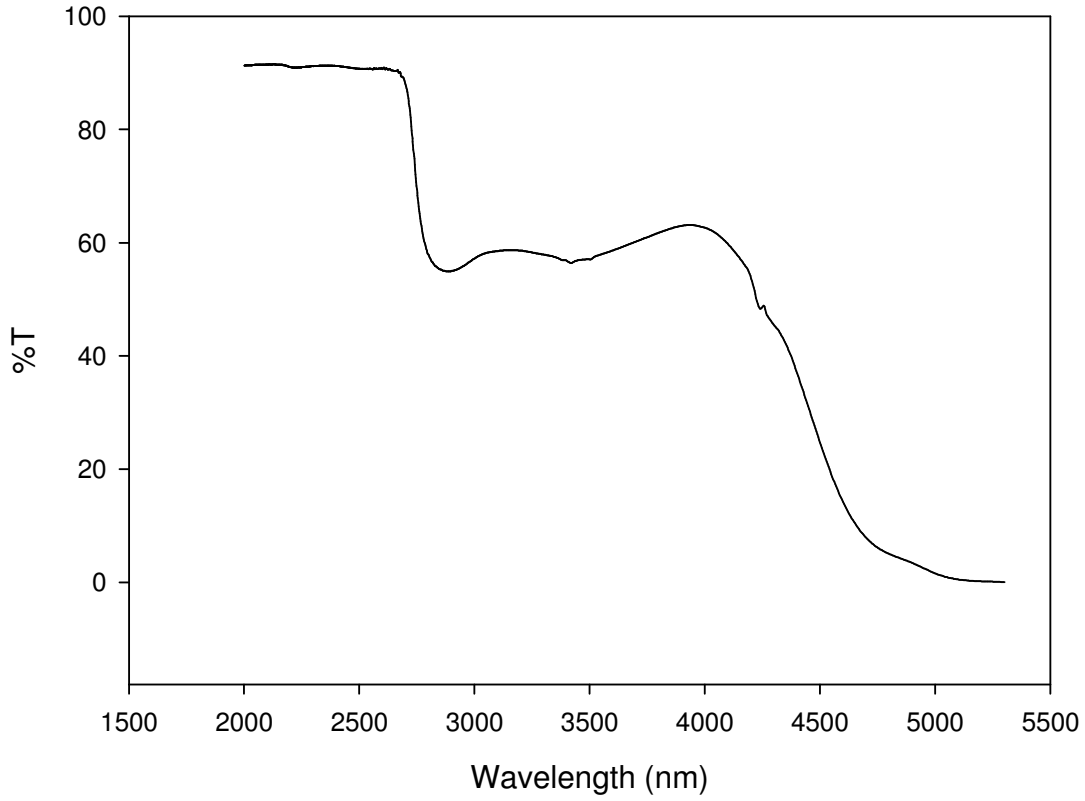

Figure 4.6 Transmittance curve for uncoated glass slide in the IR region.

A UV transmittance cut-off for both ZnO and Al_2O_3 appears to take effect at wavelength near 325 nm as shown in figure 4.7 and figure 4.11, and a sharp infrared attenuation was observed at wavelength 2700 nm and at 4100 nm where the transmittance falls to zero as can be seen from figure 4.9 and figure 4.10. These graphs come from different

measurements taken on different spectrophotometers and this is why they are given separately.

4.3.1 TRANSMITTANCE MEASUREMENTS FOR ZnO FILMS

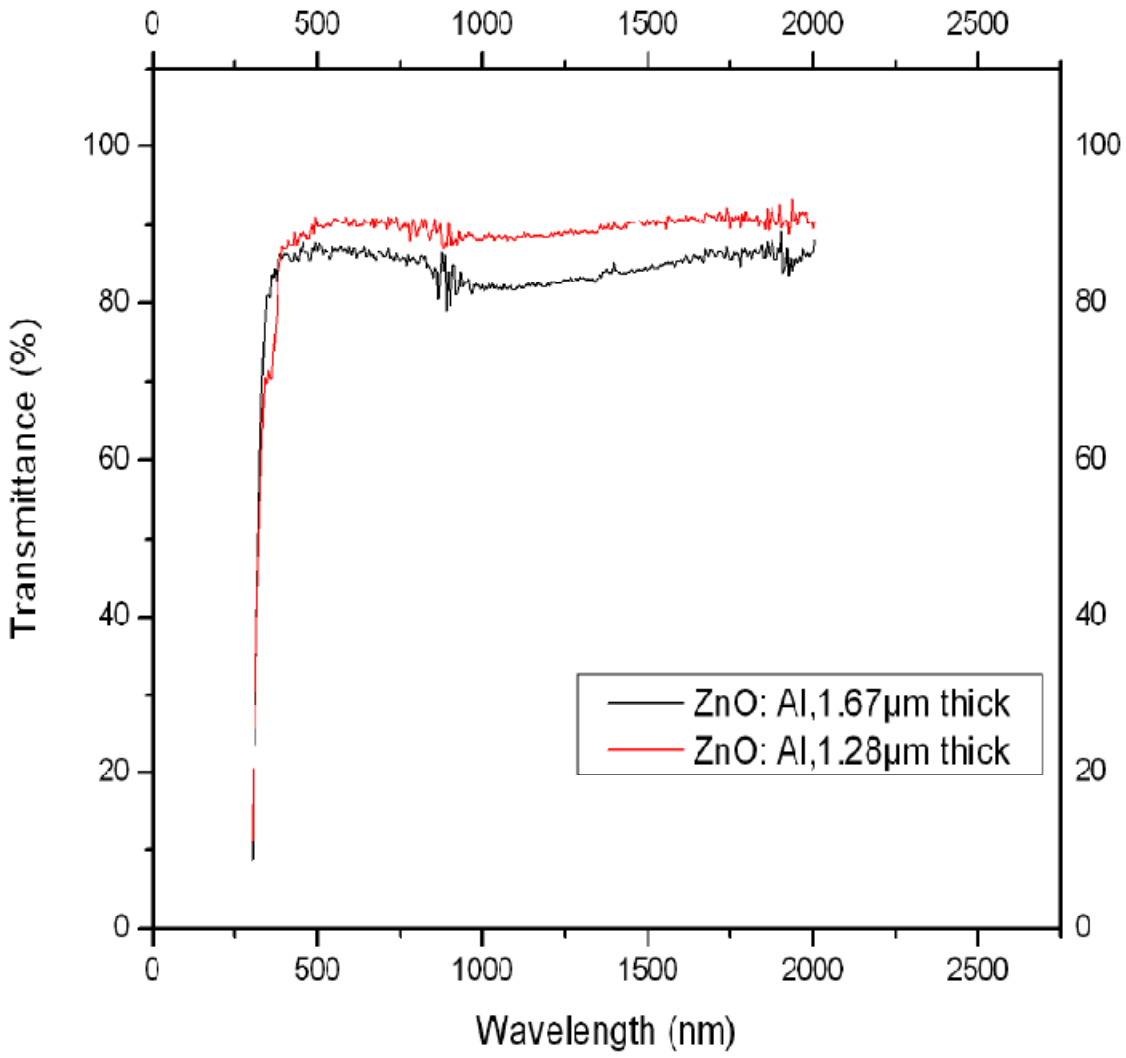

Figure 4.7 Solar transmittance curves for ZnO: Al films of thicknesses 1.67µ m and 1.28 µ m fabricated at 320^{o} C and 340^{o} C.

Figure 4.7 compares ZnO:Al thin films of different thickness. The 1.28 μm thin film gave higher transmittance values compared to the 1.67 μm thin film. This result was important because it confirmed the fact that films with lower thickness are more suited for application in thin film solar cells as transparent conducting oxides since they provide high solar transmittance. The efficiency of a thin film solar cell can greatly be improved by using TCOs of lower thickness. Figure 4.8 is another plot of the transmittance curves in the infrared region. The 1.28 μm ZnO:Al thin film still yielded better transmittance values in the NIR region but cut off the longer wavelength infrared which is not suitable for solar cell operation.

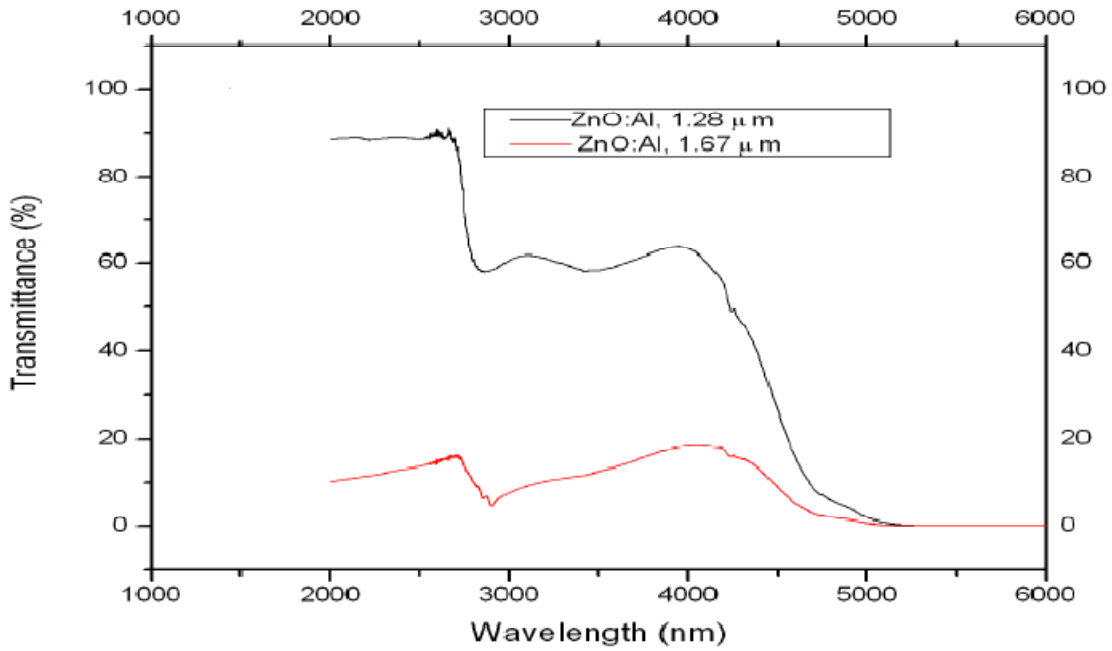

Figure 4.8 NIR and IR transmittance curves for ZnO:Al films of thicknesses 1.67μ m and 1.28 μ m fabricated at 320^{o} C and 340^{o} C.

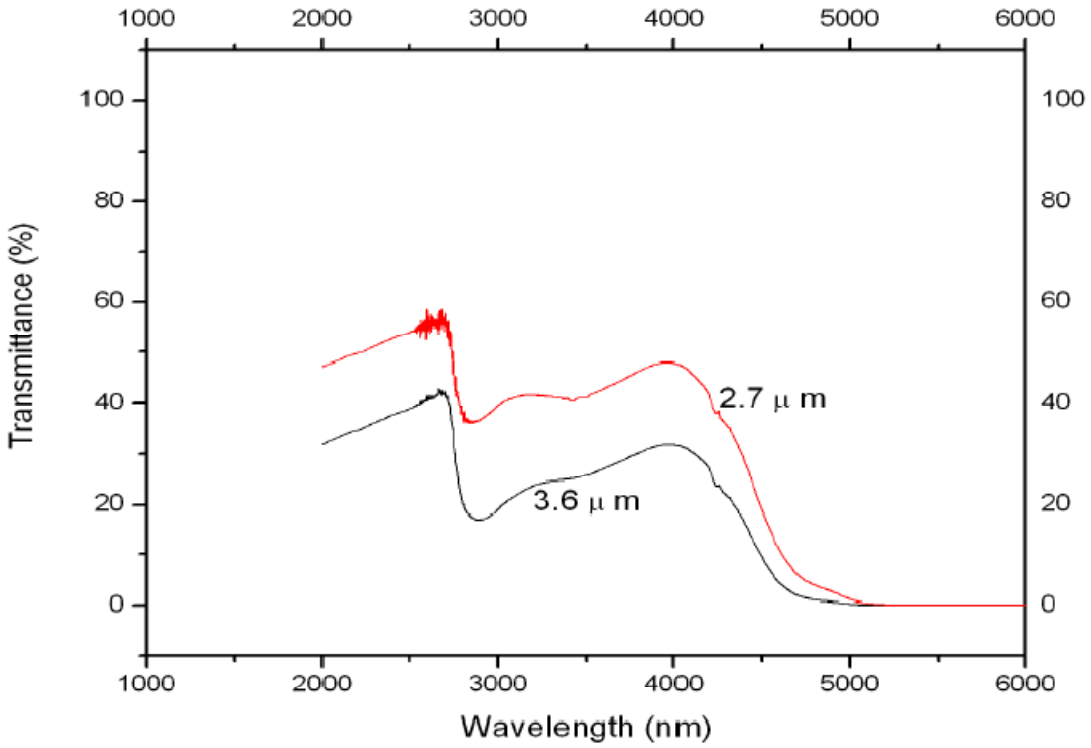

Figure 4.9 NIR and IR transmittance curves for ZnO:Al films of thicknesses 2.7 μm and 3.6 μm fabricated at 340° C and 290° C.

Figure 4.9 above provides information on the comparative transmission of ZnO:Al films of different thickness. The use of a diffused aluminium substrate for ZnO films did not produce any appreciable transmission and this can be attributed to high absorptance of the substrate. It has generally been observed that ZnO films allow more of the incident beam to be transmitted as compared to aluminium films.

4.3.2 TRANSMITTANCE MEASUREMENTS FOR Al_2O_3 FILMS

Figure 4.10 is a presentation of the transmittance curves for Al_2O_3 coatings in the NIR and FIR regions of the electromagnetic spectrum. The general picture was that there was an observed transmittance reduction at 2700 nm wavelength, reducing by approximately 20 per cent. The transmittance then remained steady between 3000 nm and 4000 nm wavelengths. After 4000 nm wavelength, the transmittance steadily dropped to zero.

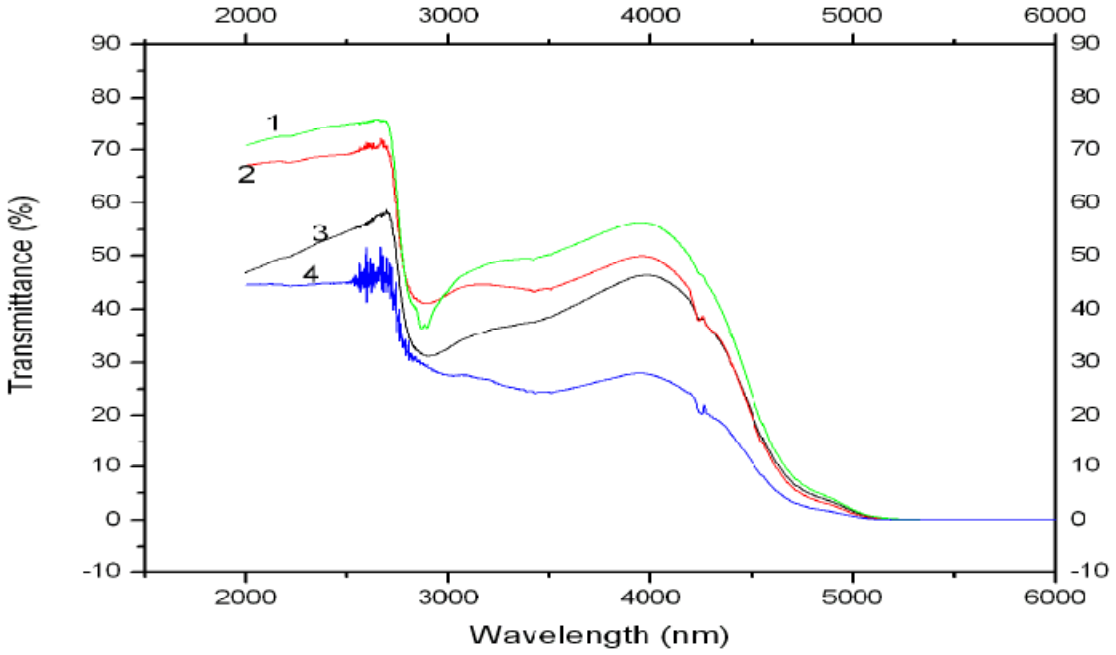

Figure 4.10 NIR and IR transmittance curves for Al_2O_3 coatings: (1) double layer undoped Al_2O_3 fabricated at 400°C, (2) Al_2O_3:Zn grown at 290°C, (3) Al_2O_3:Zn 400°C and (4) Al_2O_3:Zn 400°C.

Figure 4.11 gives the transmittance curves for the undoped Al_2O_3 thin films in the VIS-NIR wavelength region. The transmission was nearly 90 per cent. This was a good result for possible application in transparent conducting oxides for a thin film solar cell.

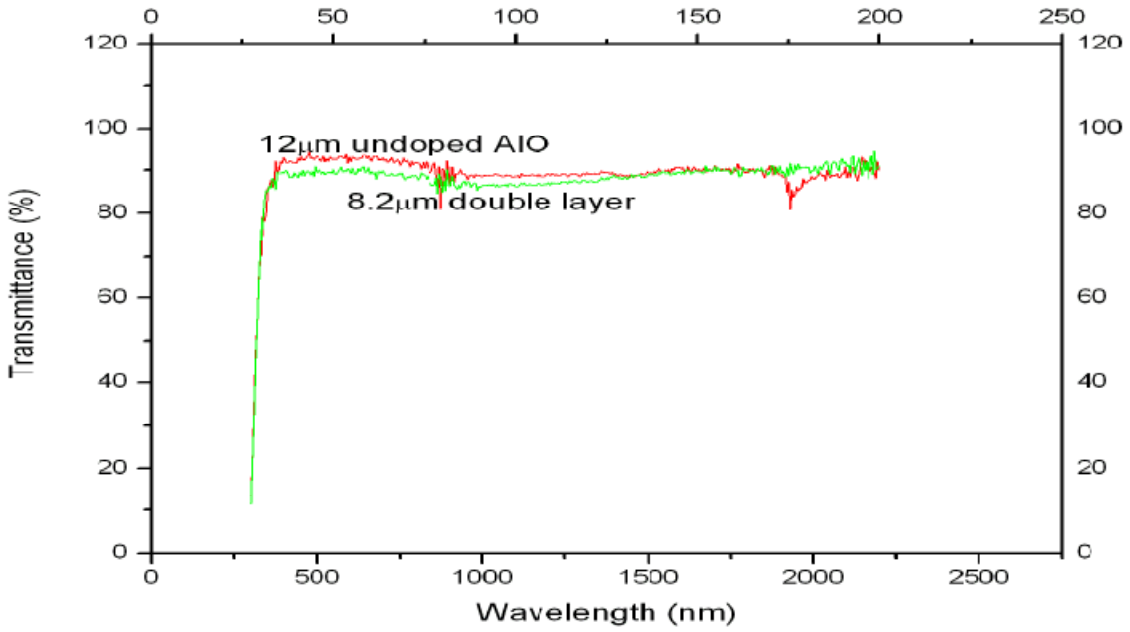

Figure 4.11 VIS-NIR transmittance of doped double layer and undoped Al_2O_3 films.

The figures above provide information on the comparative transmission of ZnO and Al_2O_3 coatings. It has generally been observed that ZnO films allow more of the incident beam of light to be transmitted as compared to the Al_2O_3 films. The highest transmittance was achieved for ZnO doped with aluminium. The percent solar transmittance was 88.03 for ZnO and 71.94 for Al_2O_3. Table 4.1 shows values obtained for different samples expressed as per-centage values. The transmittance for uncoated glass used for growing these samples was 90 per cent. This showed that very thin coatings transmit nearly like the glass on which they are coated as can be observed from the transmittance curves above. The average transmittance values in table 4.1 were computed from all the individual transmittance values in each selected wavelength range. The values were too many to be presented here in table form because they would have taken up so many pages. This is the reason why only averages have been presented.

The achieved transmittance of 88.02 per cent for ZnO films grown using spray pyrolysis method means that the thin films are suitable for use as window layers for heterojunction solar cells [59]. It means that more light is admitted to improve the performance of the solar cell. We suggest that the use of these coatings would improve the efficiency of solar cells significantly.

4.4 REFLECTANCE MEASUREMENTS

The reflectance measurement results have been corrected for the error resulting from the standard used. The standard, aluminium mirror, was 96 per cent reflecting. This meant that if the measured reflectance of any of the samples was 90 per cent, it was 90 per cent of 96.

4.4.1 REFLECTANCE MEASUREMENTS FOR ZnO THIN FILMS

Reflectance curves for selected representative ZnO thin films have been presented in figure 4.12. The observed general trend was that the reflectance peaks appear between 8,000 and 10,000 nm wavelength. In the rest of the EM spectrum, the reflectance remained relatively low.

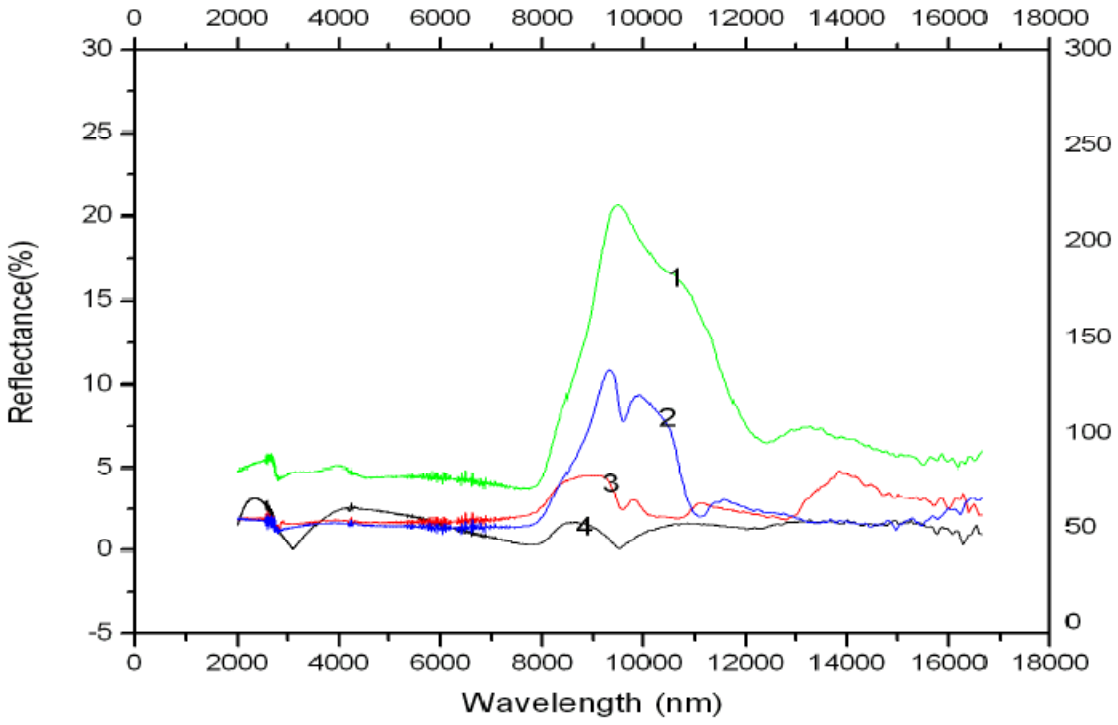

Figure 4.12 Reflectance curves for ZnO:Al. (1) 24A, (2) 25B, (3) 23A and (4) 10-03A.

The sample codes according to the labeling at the time of coating were 24A, 25B and 10-03A. Details about these samples can be found in table 4.1.

4.4.2 REFLECTANCE MEASUREMENTS FOR Al_2O_3 THIN FILMS

The reflectance observed in the Al_2O_3 coatings follow a similar pattern as that observed in the ZnO thin films. Comparatively, Al_2O_3 has slightly higher reflectance peaks in the same wavelength range compared to ZnO. The reflectance results are presented in figure 4.13.

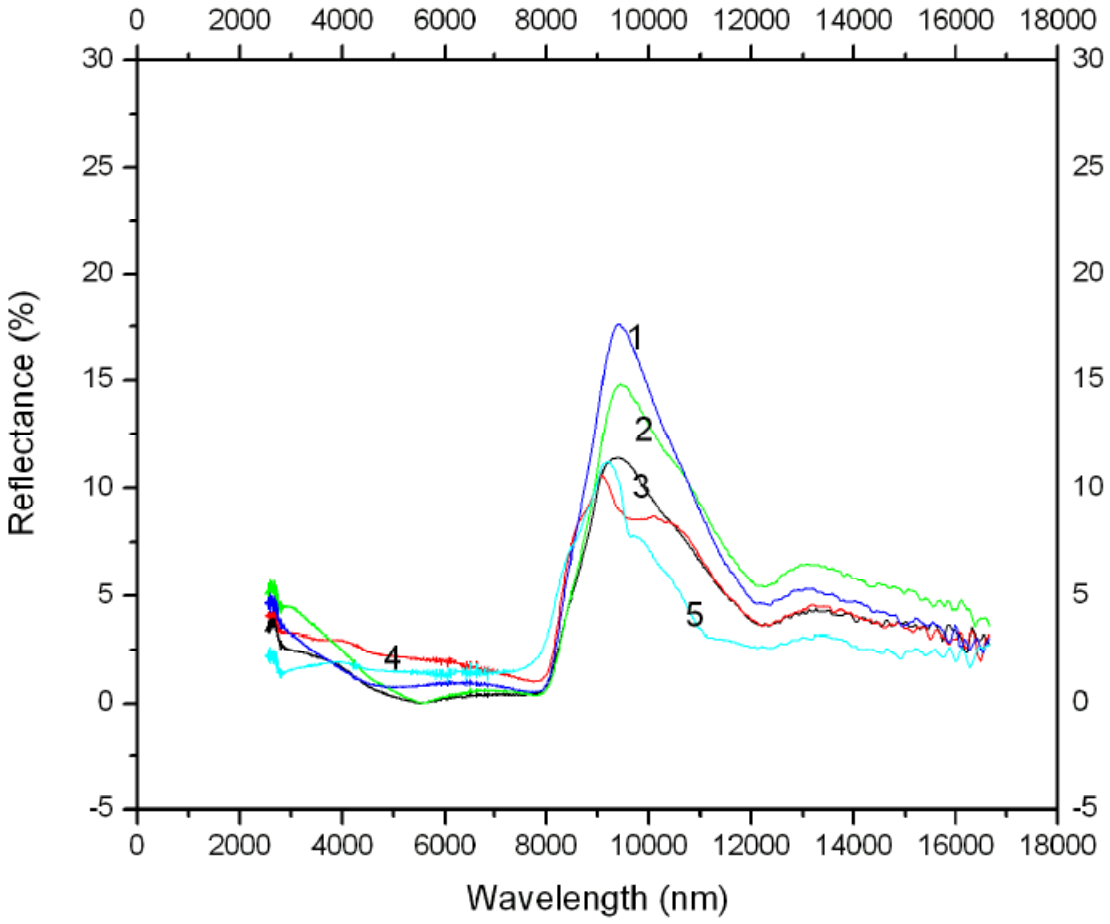

Figure 4.13 Reflectance curves for Al_2O_3: (1) 10AL,(2) S5, (3) 1A, (4) S3, (5), SC.

In general, it was observed that the reflectance results remained the same in the VIS-NIR spectrum. Therefore, the above graphs are representative of the general trends. However, the UV light is completely cut off. In all these surface coatings, the reflectance is high at 8000 nm-12000 nm wavelength window. This opens the possibility to minimize admission of this section of the infrared radiation by selective reflection using these thin films.

(Please insert table 4.1prepared separately)

Table 4.1Film growth conditions and average transmittance values.

4.5 MODELING THIN FILM PROPERTIES

This section examines experimentally derived results and uses them in theoretical models that help us to fully understand these properties and how they fit into theoretical expectations.

The wavelength-dependent refractive indices were calculated using equation (2.18). Averages were calculated for each selected wavelength range as given in table 4.1. The results were within the range of most reported results from the existing literature [60]. The resistivities of the film coatings have been evaluated from equation (2.25). For ZnO:Al the values found were 9.59 x 10^{-6} Ω m and 2.43 x 10^{-4} Ω m whereas for Al_2O_3:Zn the calculated values were 1.18 x 10^{-3} Ω m and 4.47 x 10^{-4} Ω m. The difference in the electrical properties of the two thin film oxides comes as a result of the difference in the doping levels and growth conditions. The films, though made of the same oxide, are not exactly the same. The aluminum oxide thin films have higher values than zinc oxide thin films. However, these values are lower than most reported values which are of order 10^{-4} Ω m [1]. Due to current limitation, our measurement accuracy for I-V characteristics from which the resistivity has been calculated was not that good. This was mainly attributed to poor instrument stability. This could be the major reason for the deviation in resistivity values we have reported.

Reflectance, transmittance and thickness values of the thin films have been used to calculate the absorption coefficients. The result for ZnO:Al with thickness 1.2 μm was 662.6 m^{-2} and the highest value rising to 239000 m^{-2}. This is a wide range of absorption

coefficients. They cannot be the same because they depend on the thickness of the solid thin film. The absorption coefficient has an inversely relation to the thickness of the coating but is also greatly influenced by both transmittance and reflectance values.

SPECTRUM	REFRACTIVE INDEX		
	ZnO	ZnO:Al	Al_2O_3:Zn
VIS-NIR	1.80	1.96	2.00
FIR	1.28	1.53	1.30

Table 4.2 Wavelength-dependent refractive indices of selected thin films in the VIS-NIR and FIR wavelength regimes.

In applying the effective medium theory according to Maxwell-Garnett, we considered the volumes of the medium constituents as being those of ZnO, Al_2O_3, Zn and Al particles for the doped samples. We assigned the permeability constants ε_A to aluminium atoms and ε_B to ZnO. The volume ratios and dielectric permeability constants were used in the Maxwell-Garnett effective medium approximation. Using $1.7<\varepsilon_B<2.5$ and $\varepsilon_A = 9$ in addition to the respective volumes of ZnO and aluminium, we got the effective dielectric permeability by applying equations (2.31) and (2.32). This yielded $5< \bar{\varepsilon}^{MG} \leq 6.1$ as the range of the effective dielectric permeability according to the Maxwell-Garnett effective medium approximation. The effect of doping ZnO with aluminium was that the effective permeability constant was increased and consequently

the refractive index of the film. This translates into an increased refractive index of between 2.2 and 2.4.

Application of the Bruggeman effective medium theory required the solution of the quadratic equation

$$(2+4f_A)\varepsilon^{-2Br}+(-\varepsilon_A f_A+3\varepsilon_B f_A+\varepsilon_A)\varepsilon^{-Br}+(\varepsilon_A\varepsilon_B)=0 \qquad (4.1)$$

resulting from equation (2.33) in chapter two. The solutions for ε^{-Br} were obtained after substituting for the constants ε_A, ε_B and f_A in

$$\varepsilon^{-Br}=\frac{-(\varepsilon_A f_A+3\varepsilon_B+\varepsilon_A)\pm\sqrt{(\varepsilon_A f_A+3\varepsilon_B f_A+\varepsilon_A)^2-4(2+4f_A)\varepsilon_A f_A}}{2(2+4f_A)} \qquad (4.2)$$

The composite medium constituents have been assumed to have equal probability to occupy ε_A for which the valid solutions for the effective dielectric permeability lie between 4.4 and 8.5. The resulting refractive index from this approximation lies between 2.098 and 2.91.

The graphs in figure 4.14 are optical curve fits derived from both experimental and theoretical approximations according to the Maxwell-Garnett and Bruggeman effective medium theories. Figure 4.14 combines both experimental and theoretical data fitting. Both the Bruggeman EMT and the Maxwell-Garnett have theoretical results that can be accepted within experimental error. The Mie theory has not been used for calculating effective optical and dielectric constants because of its complex nature. The figures were plotted using average values of the transmittance in the VIS, NIR and IR and the

corresponding calculated refractive indices in those spectra. The plots are for three samples that are representative of the three categories of film, which are undoped ZnO (S4), doped ZnO (26A) and doped Al_2O_3. The other samples would give similar results.

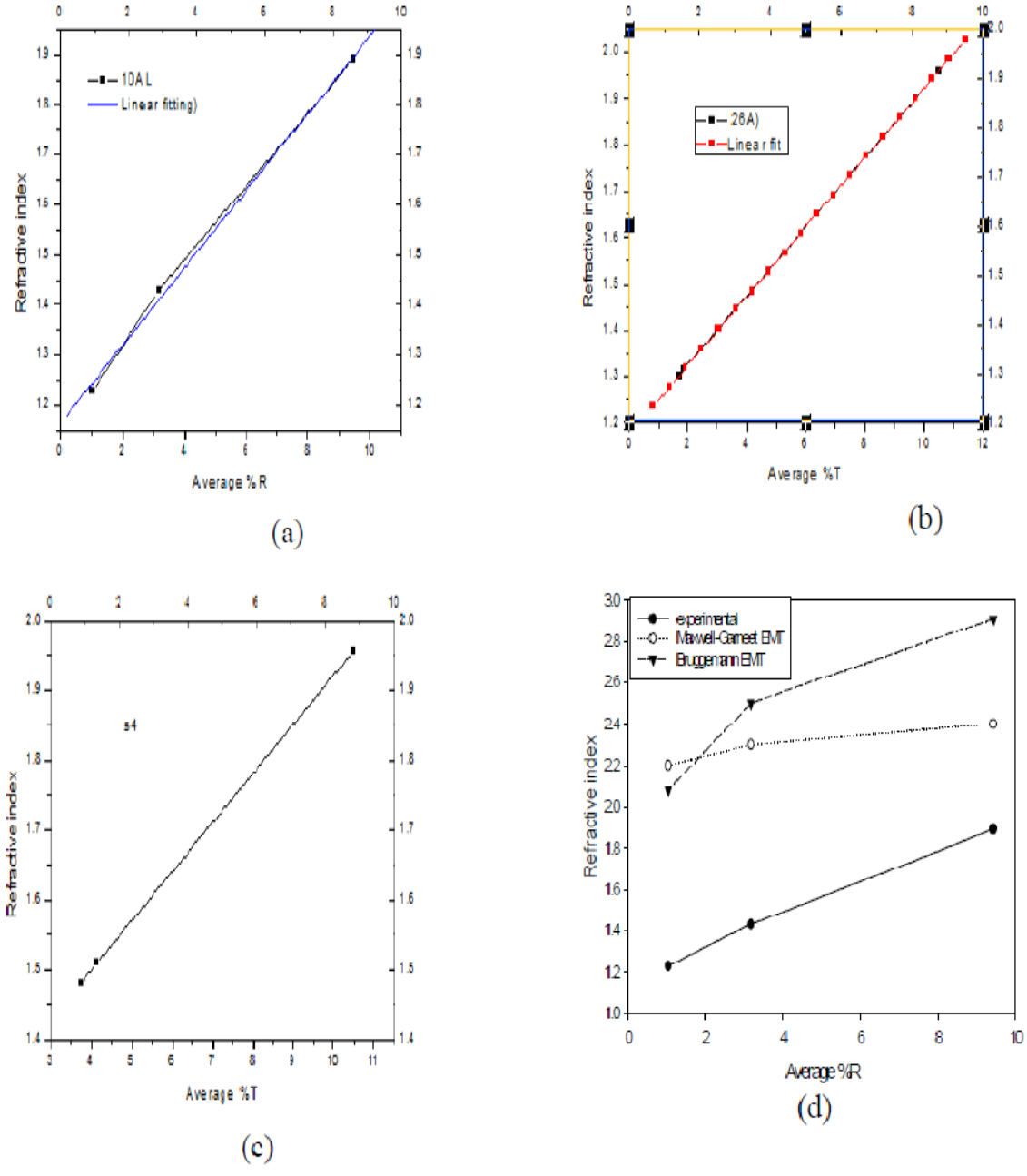

Figure 4.14 Refractive index as a function of reflectance.

4.6 SURFACE MORPHOLOGY

The analysis with the AFM revealed interesting structures of the film coatings. The roughness, cross-section and particle analyses were done for samples representing one of the five selected categories. We present here the features of each of the samples with the main emphasis being on surface roughness, surface cross-section and particle size and distribution. Figure 4.15 shows a two-dimensional scanned surface of the sample film. Some parts of the film surface in this figure appear raised up and these are indicators of the roughness of the surface. Though these cannot be seen with the naked eye, the AFM scan has revealed them. The significance of understanding the roughness is that it has an impact on the film due to the fact that the depressions minimize the effective thickness of the film and hence increase the resistance.

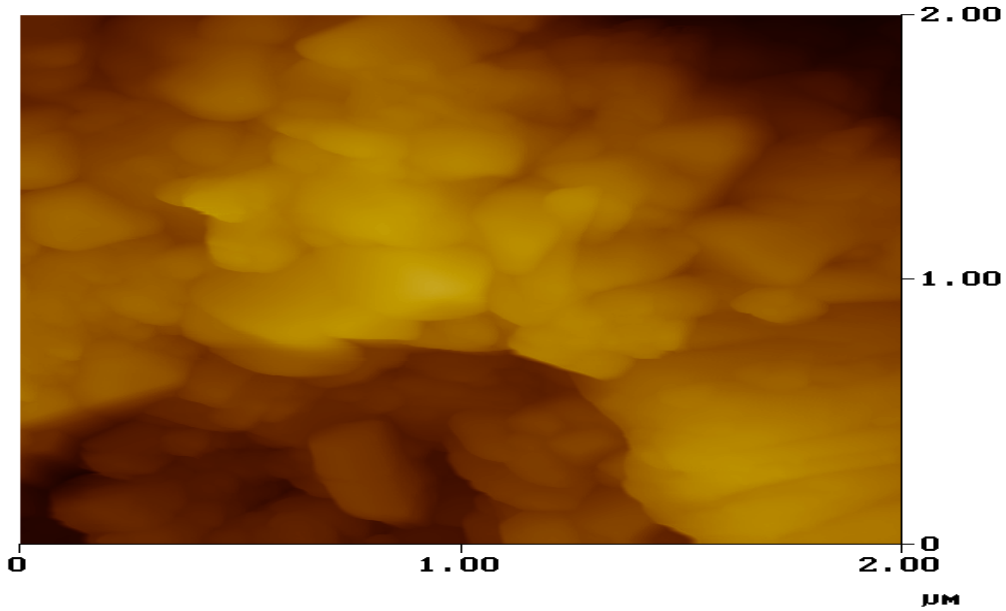

Figure 4.15 Surface roughness of ZnO doped with aluminium.

The AFM micrograph presented in figure 4.15 depicts the surface structure of the ZnO thin film doped with aluminium. The analysis indicates that the mean roughness for this particular coating was 14.11 nm. Figure 4.16 presents the cross-section analysis of the top surface of the film sample in which we notice some depressions and raised sections of the scanned area indicated by the green pointers. This is a graphical representation of the uneven top surface of the film. A section indicating some level of deformity is visible in figure 4.15, figure 4.17 and figure 4.18. In these listed figures, the lighter sections of the scan indicate a higher level surface of the coating and the dark parts signify deeper depressions. The consequence of the unevenness of the coated surface is that the thin film tends to have high sheet resistance as a result of the sections that do not have uniform thickness. This deformation gets minimized by way of multi-layer coating which results in burying the possible discontinuities and improves the thickness uniformity.

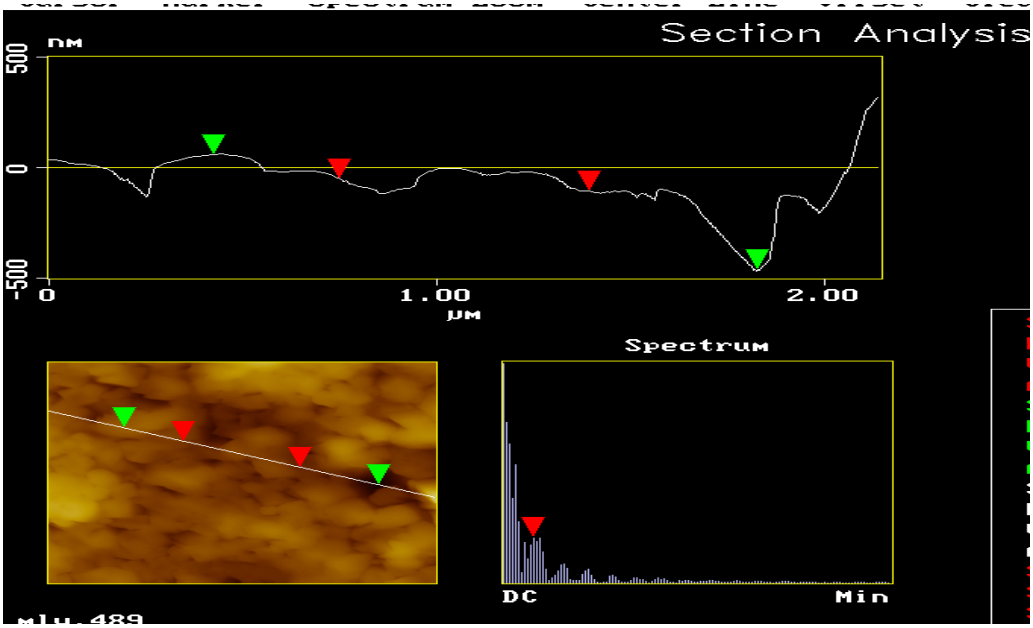

Figure 4.16 Section analysis of 3.6 μ m thick aluminium doped ZnO film deposited at 290^{o}C.

Particle size analyses of the films indicate minimum grain size of magnitude 15.259 nm^2 and a maximum size of 656.13 nm^2. It has been observed that the particle size, like other properties of the films, depends on spray parameters which include substrate temperature, spray pressure and concentration of the precursor solution. However, there is no evidence of particle size dependence on doping levels.

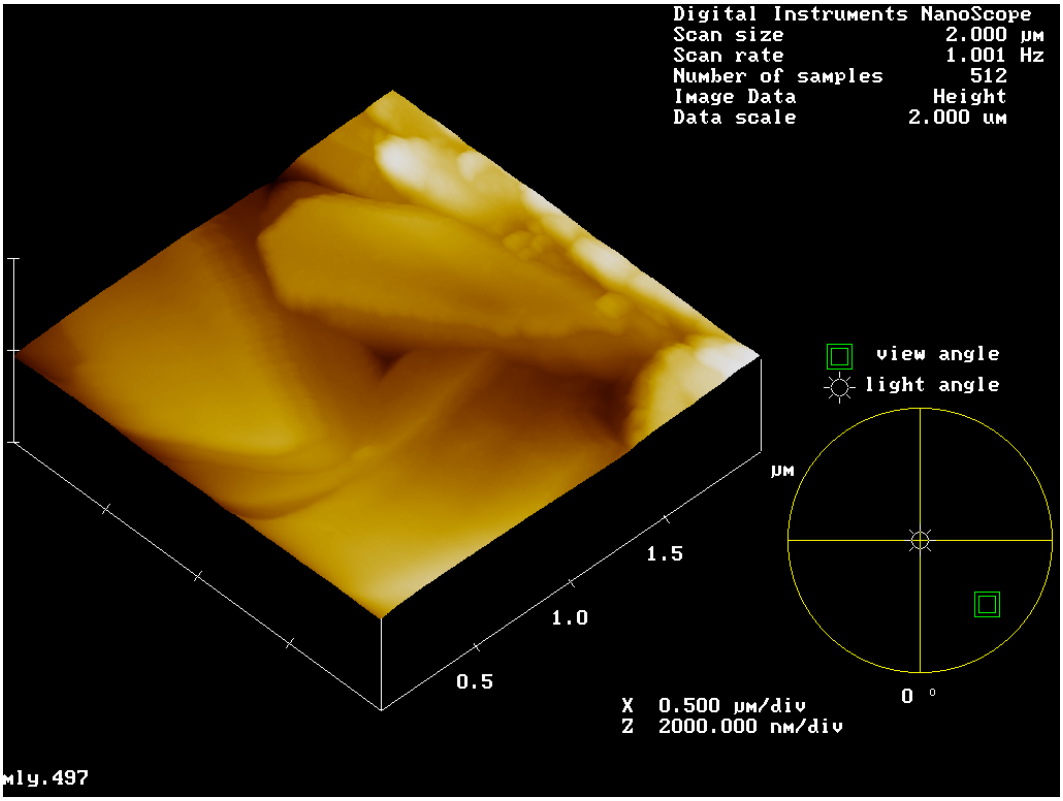

Figure 4.17 Surface plot of ZnO:Al thin film that is 0.6 μ m thick sprayed at 500kPa pressure and 340 ^{o}C substrate temperature.

Figure 4.17 above is a surface plot and roughness presentation of the 0.6 μ m thick aluminium doped ZnO thin film grown at 340^{o}C and pressure of 500 kPa. The grain sizes are large compared to those in films deposited at 290^{o}C.

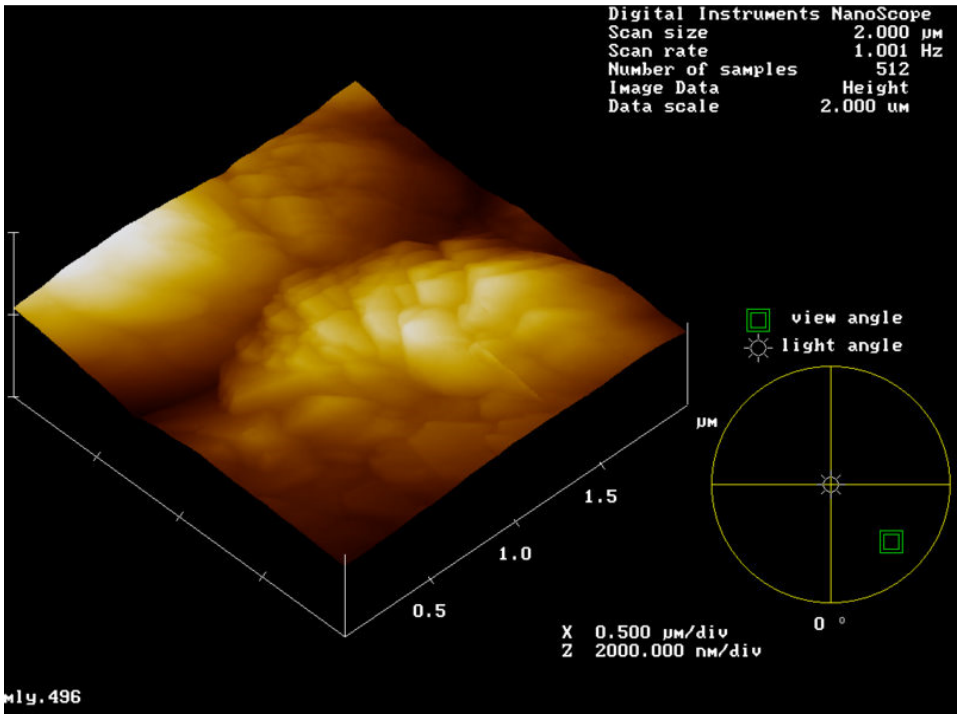

Figure 4.18 Surface plot for undoped ZnO thin film deposited at 340°C.

The films grown at temperatures ranging between 300°C and 450°C resulted in highly crystallized structures. Higher temperatures cause rapid crystallization of the precursor. Extreme temperatures could not be reached due to limitation in the heating system.

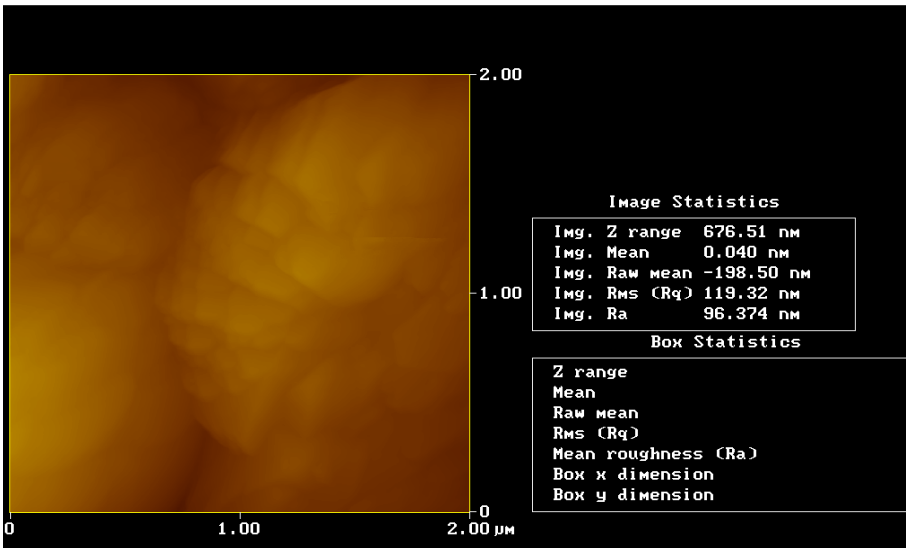

Figure 4.19 Surface roughness plot of undoped ZnO having mean roughness 96.374 nm.

Figure 4.18 is a surface plot for the undoped ZnO film. We see a slight difference in the way the surface appears. This is due to the manner in which the growth process took place as we see from the orientation of the film surface appearance. The roughness and distribution of grains are captured in figures 4.19 and 4.20 respectively.

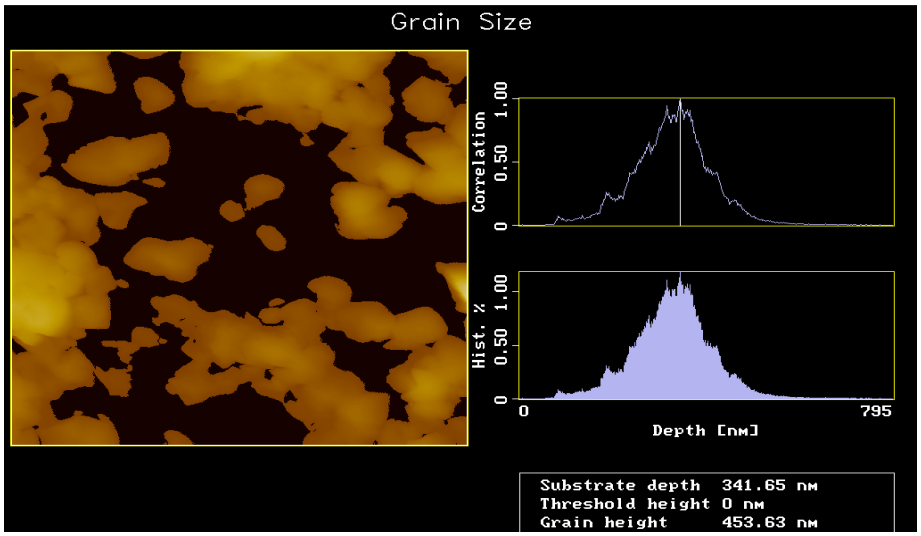

Figure 4.20 Distribution of grains in the thin film.

The black regions of figure 4.20 represent areas where the grains are absent. This is a microscopic analysis. It means that the dark areas are very small but here they appear large because of magnification.

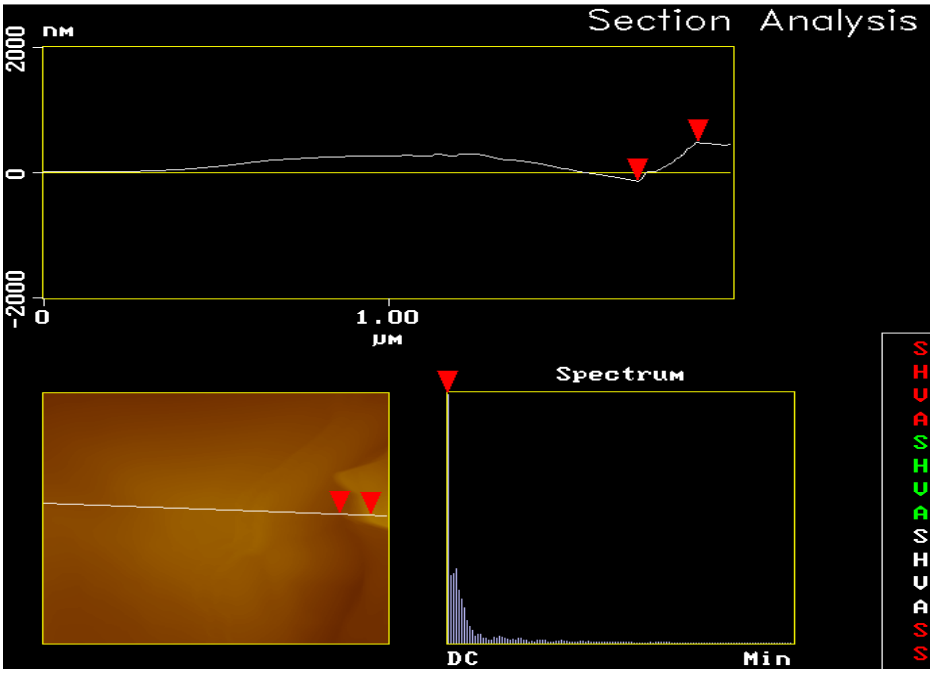

Figure 4.21 Section analysis of Al_2O_3 double layer thin film grown at 180 kPa and 400°C.

Figure 4.21 is a section analysis of the double layered Al_2O_3:Zn film. The position markers are a guide to show the sections under consideration. The line in this figure is a surface profile showing the sections with depressions. Here, the depressions are minimized largely due to doubling of the film layer. Therefore, by making double or triple layered films, the surface structure is much improved in terms of surface smoothness and evenness. This translates into improved electrical and optical properties. These films are much more suitable for solar cell transparent conducting oxides than single layered ones.

The characterization of the film surfaces has helped to correlate the surface structure to the performance of the transparent conducting thin film and consequently the performance of the solar cell. We have improved the coatings by forming double-layered structures whose sheet resistance is lower compared to single layers. This in turn has increased the likelihood of improved efficiency of the solar cell made from these films since for the same generated voltage in the cell, more current can flow. The exploiting of double coating in this work has opened room for improvement of electrical properties of the films.

4.7 ELECTRICAL PROPERTIES

Resistance values for the films were calculated from current-voltage (I-V) measurements. In this area, just representative samples were considered. Two samples were analysed for ZnO:Al and another two for Al_2O_3:Zn.

Sample	Type of film	Voltage (mV)	Current (mA)
25B	ZnO:Al	9.00	6.00
26A	ZnO:Al	7.00	0.47
S5	Al_2O_3:Zn	4.00	0.36
10-03A	Al_2O_3:Zn	4.80	0.20

Table 4.3 I-V characteristics of ZnO:Al and Al_2O_3:Zn thin films.

4.7.1 ELECTRICAL PROPERTIES OF ZnO:Al THIN FILMS

The selected samples in this category are 25B and 26A. The sheet resistance of the ZnO:Al thin films and the corresponding resistivity were calculated and tabulated in table 4.4 below.

Sample	Resistance (Ω)	Average resistance (Ω)	Resistivity ($10^{-4}\ \Omega$ m)
25B	0.75	5.24	0.0959
26A	9.54		2.43

Table 4.4 Calculated electrical values for ZnO: Al.

These values were calculated using equation (2.29) and equation (2.30) from chapter two. The electrical results are suitable for application of these films in thin film solar cells [21].

4.7.2 ELECTRICAL PROPERTIES OF Al_2O_3:Zn THIN FILMS

In a similar manner, the sheet resistances for Al_2O_3:Al thin films were calculated from I-V characteristics. The film resistance and resistivity values obtained by application of equation (2.29) and equation (2.30) for selected films are given in table 4.5. The

resistivity values obtained for both zinc and aluminium oxide thin films were within the range of some reported values [1,8].

Sample	Resistance (Ω)	Average resistance(Ω)	Resistivity (10^{-4} Ω m)
S5	5.56	8.78	11.8
10-03A	12		4.47

Table 4.5 Calculated electrical values for Al_2O_3:Zn thin films.

CHAPTER V

DISCUSSION AND CONCLUSION

5.1 DISCUSSION

Solid thin films of zinc oxide doped with aluminium and films of aluminium oxide doped with zinc have been characterized for their structural, electrical, surface and optical properties. In the spray process, the films were allowed to grow at the centre of the substrate thus forming a circular disc. This was helpful when it came to determining the thickness by the step method using the Tencor Alpha Step Profiler. The recorded thickness was a profiled vertical difference between the top surface of the solid film and the contact the film made with the substrate. It is experimentally difficult to create a step in spray pyrolysis by covering part of the substrate. The reason is that in this method, one is dealing with liquid substances that can easily sip through the created barrier and no meaningful step is achievable. The height profile was traced by the stylus of the profiler. We observe from figures 4.4 and 4.5 that the steps were not distinctly sharp but were characterized by steady slants with periodic depressions, some of which have been attributed to stylus dig out as the instrument scanned through the surface of the film. As a result of this possible scratching of the film surface by the profiler, precautionary measures were taken not to scan the same section for the surface morphology.

The other area of great interest was the temperature distribution in the furnace but most importantly on the substrate. The temperature was monitored with a calibrated

thermocouple that produced results within the set tolerance (acceptable variation in temperature) of 20^0C. Growth of the films was done at temperatures ranging from 240^0C to 500^0C. It must be noted that this was also the temperature range for the experimental setup as limited by the available heating elements. In this temperature range, acceptable qualities of zinc oxide and aluminium oxide coatings were obtained. The best results in terms of quality were obtained at temperatures between 300^0C and 400^0C. An attempt to produce films in another Carbolite oven at higher temperatures did not give improved results. The films produced were powdery. This phenomenon could have been caused by rapid evaporation of the precursor solution, which turned solid before achieving strong adhesion with the glass substrate. The other constraint with the Carbolite oven was that it was not possible to get the configuration or assemble the apparatus the way we would have liked because its in-built structure could not be changed.

It was noted during transmittance measurements that the UV spectrum was not transmitted. Moving further, the transmission of the electromagnetic waves attenuated at wavelength 3000 nm and attenuated further to a minimum value at wavelength 4500 nm. This was true for both types of films. This confirmed the spectrally selective transmission nature of the thin films. In a similar manner, notable selective reflection was observed. The reflection in the VIS-NIR was minimal. Reflectance amplitudes were observed between 8,000 nm and 10,000 nm. This means that the films produced in this project were spectrally selective and therefore offer an alternative to ITO for application as transparent conductors in thin film solar cells. The spectrally selective property confirmed in these thin films is important for TFSC application since their transmittance

is high in the VIS-NIR wavelength region which is an important section of the spectrum for effective performance of the cells. It has been confirmed also that these films cut off the far infrared, which degrades the performance of the cells.

Since transmission is high for both types of film in the solar spectrum, it is safe to say that these thin films can be applied as transparent conducting coatings on thin film solar cells as well as in other applications that require high transmission in the solar spectrum. They can also be applied to minimize transmission in the far infrared spectrum.

Generally, the results obtained and presented are promising for application in solar cells. We have obtained transmittance values that have improved by 5 per cent from those recorded in previous measurements [7, 20], and with these values we expect a slight improvement in the efficiency of the solar cell due to more light reaching the absorber. An observation has been made on the high reflectance of the unwanted infrared wavelengths for both types of film with a reflectance peak lying between 8000 nm and 10,000 nm wavelengths. This high reflectance offers an opportunity for application of the thin films in other devices where infrared radiation of this wavelength range is unwanted. The result presents an opportunity for further investigation so that rejection or transmission of the electromagnetic waves at this wavelength range can be further investigated for possible application in some devices.

The electrical properties obtained were close to those presently recorded in most of the reported works [7, 13, 20, 21]. Lower resistivity values have been achieved in this

project. It is proposed that achieving lower resistivity values raises the conductivity of the solar cell materials and hence leads to improved cell performance and conversion of solar energy to electrical energy. On the other hand, we have worked to improve the film morphology by application of double coating techniques. This resulted in improvement in the uniformity of the film surface and hence increased solar transmittance. In this coating method, we have seen that it is possible to obtain very thin films for various applications, a case which may not be true in many other film growth techniques.

The results obtained have direct impact on the performance of the thin-film solar cells. Low thicknesses, high transmittance of VIS-NIR, high reflectance of FIR, good electrical and uniform surface morphology translate to a high-performance thin-film solar cell when all these properties are optimized in the cell. When these results are compared with the properties of ITO, we see that the transmittance and electrical conductivity offered by the ZnO:Al films are in the same range i.e., 90 per cent transmittance in the solar spectrum and electrical resistivity of the order of $10^{-4}\,\Omega\,\mathrm{m}$. This means that ITO can be replaced by ZnO:Al thin films at a reduced price. On the other hand, the transmittance of Al_2O_3:Zn is fairly good and its resistivity falls in the same range as tin-doped indium oxide. The effect of doping has led to increased transmittance and reduced resistivity, thus leading to well performing solar cells when they are used as TCOs in the solar structure.

This work has presented a new way of looking at the growth of thin films for solar energy applications. The first innovation applied here is the use of mutual doping of zinc

and aluminium oxides. The zinc oxide was doped with aluminium to produce ZnO:Al solid thin films while on the other hand aluminium oxide has been doped with zinc to produce Al_2O_3:Zn film coatings. Previous research work involved doping with indium and nitrogen [13]. The properties of both types of film have been studied. A survey of previous works on thin film materials has shown that most researchers concentrate on investigating only a few properties of their surface coatings. In our work, we have made an attempt to investigate all the properties relevant to thin-film solar cell performance and have proceeded to model these properties with effective medium theories. The properties we have investigated have been related to solar cell performance in chapter four, and how each property influences the performance has been stated. For example, high solar transmittance leads to generation of more charge carriers and low resistivity leads to high conductivity. Another new aspect is the use of cheap and locally available raw materials, namely zinc chloride and aluminium chloride hexahydrate, which were dissolved in cheap and readily available distilled water as the solvent. The initial proposal was to dope with indium but this was found to be expensive and already widely covered by other researchers. The coating unit used was locally constructed at the University of Zambia [34]. This was improved to suit this work by introducing asbestos coverings on the walls, and an easy way of temperature monitoring using a calibrated nickel-chromium thermocouple was employed. For characterization, standard techniques have been used to determine the properties of the film coatings and the results obtained have been used to model the effective properties using Maxwell-Garnett and Bruggeman effective medium theories.

An additional hypothesis to the one we have considered in this dissertation, which we would have liked to have tested, is that zinc and aluminium nano-particle oxides are good raw materials for growth of thin films for solar energy absorbers. But due to limitation in the experimental apparatus, namely the blocking of the capillary of the atomizer, we could not test this hypothesis.

5.2 CONCLUSION

In this study, we have utilized a simple and cheap process of fabricating spectrally selective thin solid films by way of the spray pyrolysis process. Process parameters were easy to control with the ability to coat large surfaces. The films' optical, electrical and structural properties have been investigated. An improvement of up to five per cent in the transmittance has been achieved. Further, low electrical resistivity values have been obtained which are promising for applications in thin-film solar cells. A new transparent conducting thin film combination in solar cells has been proposed. This is the use of a ZnO:Al/Al_2O_3:Zn TCO combination to replace the ITO/SnO_2 combination. In this combination, the materials used give good results as ITO with an expected improvement in the efficiency at a much cheaper cost. A wide range of properties were investigated. Efforts were made to optimize the process of coating the films by varying the growth parameters. Cheaper and locally available raw materials were used as a measure to lower the production cost of thin-film solar cells. Standard effective medium theories for thin film modeling were applied to obtain effective refractive and dielectric permeability constants.

A solar transmittance of 88 per cent was obtained for doped zinc oxide and 71.9 per cent for aluminium oxide films. This result is good for thin film application in solar cell manufacture because more light is allowed onto the active section of the cell and in turn more charge carriers are generated in the process. Reflectance values in the solar spectrum remained below 20 per cent with minimal absorption, except for slightly thicker aluminium oxide coatings. In the infrared region, reflectance peaks were observed in the wavelength range 8,000-13,000 nm as seen in figure 4.12 for ZnO and figure 4.13 for Al_2O_3 coatings. The films produced in this undertaking were spectrally selective. The ZnO:Al/Al_2:Zn are spectrally selective films. This means that when they are used as TCOs in solar cells, they would block unwanted frequencies, especially those lying outside the solar spectrum. This is good for solar cells because unwanted electromagnetic wavelength regions are blocked and this prevents solar cell degradation. There was complete cut off of the UV light having wavelength below 300 nm. Transmittance was high in the VIS-NIR wavelength region while the FIR wavelength region was partly reflected and partly absorbed. The wavelength-dependent refractive indices were calculated from experimental results. In the VIS-NIR region, values of 1.96 for the refractive index of doped zinc oxide and 2.0 for that of aluminium oxide were obtained; these dropped to 1.53 and 1.3 in the far infrared region respectively. The thickness of the film coatings produced in this work ranged between 0.14 and 87.7 μm. The low thickness values are important in reducing absorption by the transparent conducting oxide in a solar cell. Electrical and structural properties (uniformity and thickness) were investigated and the film resistivities obtained were to the order of 10^{-4} Ω m. This result was good for possible application in thin film solar cells since lower

resistivity values translate to high electrical conductivity. A way to improve the surface morphology of the film coatings has been established. This is achieved by double or triple coating to bury the deformities that result when a thin film is made of a single coating. The Maxwell-Garnett and Bruggeman effective medium theories were applied to obtain effective dielectric permeabilities of the film coatings. The Maxwell-Garnett EMT produced a dielectric permeability range of 5-6.1 and the Bruggeman approximation yielded values of 4.4-8.5. These values indicated that doping ZnO with aluminum raised its dielectric permeability and also raised the refractive index. The high dielectric permeability may adversely affect the electrical conductivity of a material. Similarly, high values for the refractive index may lower the transmittance of light in a given material. However, the results obtained in this research show that the dielectric permeabilities are relatively low. On the other hand, doping has resulted in slight increases in the dielectric and refractive index properties to bring these values to a desirable level. With these values we expect good performance.

These results show that doped oxide thin films of zinc and aluminium make good transparent conducting oxides which offer a good and cheap alternative to ITO in the manufacture of cheaper thin film solar cells.

5.3 SUGGESTIONS FOR FUTURE WORK

There are many areas in which these thin films can be applied. However, there is need for further investigation of the reflectance peaks at 10μm wavelength. There is also need to make Hall effect measurements to fully establish the electrical conductivity of

charge carriers, that is, electron and hole mobility. Last but not the least, the stability of these thin films when exposed for a long time to the environment needs to be investigated. The same needs to be done for their durability under various climatic conditions.

REFERENCES

[1] K. L. Chopra, P. D. Paulson and V. Dutta, *Thin Film Solar Cells: An Overview*, Progress in Photovoltaics: Research and Applications. (2004), **Vol. 12**, pp 69-92.

[2] C.M. Haanyika , *Energy Policy,* Elsevier Journal, (2008), **Vol.36**, pp 1044–1058.

[3] Ministry of Energy and Water Development, *Zambia: National Energy Strategy*: *2008-2030,* Zero Draft, (2008).

[4] G. W. Mbise, *Optical Materials and Solar Energy Applications*, Ninth College on Thin Films, **Vol. 9.4**, July 24 – August 4, (2006), University of Dares salaam, Dar es Salaam, Tanzania**.**

[5] C.G. Granqvist, *Spectrally Selective Surfaces for Heating and Cooling*, (1979), SPIE Optical Engineering Press, Bellingham, USA.

[6] http://en.wikipedia.org/wiki/electromagnetic_spectrum.

[7] J. M. Ting and B. S. Tsai, *Materials Chemistry and Physics*, (2001), **Vol. 72 (2)**, pp273-277.

[8] G. Haacke, *Transparent Conducting Coatings,* Annual Review Matter Science, (1997)**, Vol. 7**, pp. 73 – 93.

[9] http://www.cerac.com, CERAC Inc. technical publications, *Tin-Doped Indium Oxide for Optical Coatings*.

[10] http://en.wikipedia.org, free encyclopedia, *Indium Tin Oxide*.

[11] J.H. Kim, V. I. Bashok, T. A. Germer, J. W. Mulholland and S.H. Ehrman, *Co-solvent Assisted Spray Pyrolysis for the Generation of Metal Particles*, Journal of Material Research, (2003), **Vol. 18, No. 7**, pp 1614-1622.

[12] C. E. Morosanu, *Thin Films by Chemical Vapour Deposition,*(1990), Elsevier journal.

[13] Sonny Xia-zhe Li, *Nitrogen doped zinc oxide thin films*, M.Sc. dissertation, University of California, (2000), California, USA.

[14] I. Asimov, *Isaac Asimov's Book of Facts*, (1992), Hastingshouse/Daytrips Publ., p389.

[15] Wontae Cho, Kiwhan Sung, Ki-Seok An, Sun Sook Lee, Chang G.Kim and Yunsoo Kim, *Preparation of Thin Films and Nanoparticles of Zinc Oxide using Alkylzinc Alkoxides,*KRICT, Korea.

[16] S. Y. Lee, E. S. Shim, H. S. Kang, S. S. Pang, and J. S. Kang, *Thin Solid Films*, (2005), 437, 31**.**

[17] M.P.Sing, T. Shripathi and S.A Shivashankar, *Aluminium Oxide Thin Films Grown by Low PressureMOCCVD using Aluminium Acetylacetone and Nitrous Oxide,* http://www.electrochem.org.

[18] Jinhui Mao, Bingchu Cai, Maosong Wu and Guoping Chen, *Deposition of Aluminium Oxide Films By Pulsed Reactive Sputtering,* Journal of Material Science and Technology, (2003), **Vol. 19, No. 1**, pp 368-370.

[19] Jaehyoung Koo, Janghee Lee, Seokhoun Kim, Young D. Kim and Hyeongtag Jeon, *Hafnum-Aluminum-Oxide Thin Films Deposited using Atomic Layer Deposition with Various Aluminum Compositions,* Journal of the Korean Physical Society, (2003), **Vol**. **47, No. 3**, pp 501-507.

[20] Hyeong Joon Kim,_ Sang Yong No, Dail Eom and Cheol Seong Hwang , *Property Improvement of Aluminium-Oxide Thin Films Deposited under Photon Radiation by*

Using Atomic Layer Deposition, Journal of the Korean Physical Society, (2006), **Vol. 49, No. 3**, pp. 1271_1275.

[21] A.R. Hind and Lissete Chomette, *The Determination of Thin Film Thicknes using Reflectance Spectroscopy*, Varian UV At Work, **No. 090**.

[22] H.J. Möller, *Semiconductors for Solar Cells*, (1993), Artech House Inc., London, UK.

[23] T. David, S. Goldsmith and R. L. Boxman, *Dependence of Zinc Oxide Thin films Properties on Filtered Vacuum Arc Deposition Parameters,* **Tel Aviv 69978**, Tel Aviv University, Tel Aviv, Israel.

[24] M.Kon, P.K. Song, Y.Shigesato, A. Mizukami and K.Suzuki, Japanese Journal of Applied Physics, (2002), **Vol. 41**, pp 814-819.

[25] Haiying Chen, Chengfeng Qiu, Huajun Peng, Zhilang Xie, Man Wong and H.S. Kwok, *Co-sputtered Doped Zinc Oxide Thin Films as Transparent Anode for Organic Light-emitting Diodes*.

[26] K. Krunk, O. Bijakina, V. Mikli, T. Varema and E. Mellikov, *Zinc Oxide Thin Films by Spray Pyrolysis,* Physica Scripta, (1999), **Vol. T79**, pp 209-212.

[27] D. Perednis and L.J. Gaucker, *Thin Film Deposition by Spray Pyrolysis,* Journal of Electroceramics, (2005), **Vol. 14**, pp 103-111.

[28] M. Krunks, E. Bijakina, T. Varema and D. Meisues, *Optical Organic and Semiconductor Inorganic Materials*, Proc. SPIE, Washington, **Vol. 968**, p129.

[29] J. Hirunlabh, S. Suthateeranet, K. Kirtikara and R. D. Pynn, *Development of Spray Pyrolysis Coating Process for Tin Oxide Film Heat Mirrors*, Thamasat International Journal of Science and Technology, (1998), **Vol.3, No.2**, pp. 10-20.

[30] J. C. Viguie and J. Spitz, *Chemical Vapour Deposition at Low Temperature*, J. Electrochem. Soc. (1975), **Vol. 122**, pp 585-588.

[31] A. Tiburcio-Silver, A. Sanchez-Jaurez and A. Avila-Garcia, *Solar Energy materials*, (1998), **Vol. 55**, **No. 3**.

[32] D. Todorovsky, R. Todorovska, N. Petrova, M. Uzunova-Bujnova, M. Milanova, S. Anastasova, E. Kashchieva and S. Groudeva-Zotova, *Spray-Pyrolysis, Deep-And Spin-Coating Deposition of Thin Films and their Characterization*, Journal of University of Chemistry, Technology and Metallurgy, (2006), **Vol. 41**, **No. 1**.

[33] Horea Iustin NAŞCU and Violeta POPESCU, *CuS Thin Films Obtained by Spray Pyrolysis,* Leonardo Electronic Journal of Practices and Technologies, (2004), **ISSN 1583-1078**, PP. 22-29.

[34] F. D. Phiri, *The Construction of the Heating System for the Spray Pyrolysis Oven,* P495 project report, University of Zambia, (2003), p 7-8, Lusaka, Zambia.

[35] D. Perednis and L. J. Gauckler, *Thin Film Deposition Using Spray Pyrolysis,* Journal of Electroceramics, (2005), **Vol. 14**, pp. 103-111.

[36] http://physics.tamuk.edu/~suson, *Propagation of Light using electromagnetism*, pp.1-14.

[37] Milton Ohring, *Materials Science of Thin Films, Deposition and Structure*, (2002), 2nd ed, Academic Press, San Diego, USA.

[38] B. Altiokka and S. Aksay, *Optical Properties of $CuInS_2$ Films Produced by Spray Pyrolysis Method,* Journal of Arts and Sciences, (2005), **Vol. 3**, pp.28-30.

[39] T. David, S. Goldsmith and R. L. Boxman, *Dependence of Zinc Oxide Thin films Properties on Filtered Vacuum Arc Deposition Parameters,* **Tel Aviv 69978**, Tel Aviv University, Tel Aviv, Israel.

[40] Bertil Stjema, *Electrical and optical properties of doped tin oxide films*, Ph.D. thesis, (1992), University of Goteborg, Goteborg, Sweden.

[41] F. A. Jenkins and H.E. White, *Fundamentals of Optics*, 4th ed., (1981), MacGraw-Hill Inc.

[42] J. Chan, *Four-Point Probe Manual,* (1994), EECS 143 Micro fabrication Technology, USA.

[43] K. D. Schroder, *Semiconductor Materials and Device Characterization,* (1998), 2nd Ed. John Wiley and Sons, NY, USA.

[44] V.E. Henrich, P.A. Cox, *The Surface Science of Metal Oxides*, (1994), Cambridge University Press, Cambridge.

[45] S. Berthier and J. Lafait, *Effective Medium Theory: Mathematical Determination of the Physical Solution for the Dielectric Constant,* Optics Communications, (1980), **Vol. 33**, **No. 3**, pp 303-306.

[46] A. H. Shivora and J. A. Kong, *Effective Permeability of Dielectric Mixtures,* IEEE Transactions on Geoscience and Remote Sensing, (1988), **Vol. 26**, **No, 4**, pp 420-429.

[47] D. M. Wood and N. W. Ashchroft, Effective Medium Theory of Optical Properties of Small Particle Composites, Philosophical Magazine, (1977), **Vol. 35**, **No**, **35**, pp 269-280.

[48] A. Bittar, S, Berthier and J. Lafait, *Non-metal-metal Transition in Bruggeman Optical Theory for Inhomogeneous Media,* Journal de Physique, (1984), **Vol. 45**, pp 623-631.

[49] H. Weissker, J. Furtmuller and F. bechstedt, *Validity of effective-medium theory for optical properties of embedded nanocrystallites from nab initio supercell calculations,* Physics Review, (2003), **B67,** 165322, pp. 1-6.

[50] T. C. Choy, *Effective Medium Theory, Principles and Applications,* (1999), Oxford University Press, UK.

[51] J. R. Frisvad, N. J. Christensen and H. W. Jensen, Computing the scattering Properties of Participating Media using Lorentz-Mie Theory, ACM Transactions on Graphics, SGGRAPH 2007.

[52] T. B. Chibuye, *A Comparative Study of Copper-and Nickel-Pigmented Anodised Aluminium Coatings for Solar Energy Absorption,* PhD thesis, (2004), University of Zambia, Lusaka, Zambia.

[53] G. A. Niklasson, C. G. Granqvist and O. Hunderi, *Effective medium models for the optical properties of inhomogeneous materials,* Applied Optics, (1981), **Vol. 20 No. 1,** pp 26-30.

[54] http://www.pil.uni-stuttgart.de/glossar/EffMedium_e.php, *Effective Medium Theory*

[55] B.L. Theraja, *Modern Physics*, (1999), S. Chand and Company LTD, New Delhi, India.

[56] S. Berthier, *Anisotropic Effective Medium Theories***,** Journal de Physique Internationale de France, (1994), **Vol. 4**, pp 303-318.

[57] http://cfnewsads.thomasnet.com/images.

[58] http://www.irina.eas.gatech.edu, *Scattering and Absorption by Aerosol and Cloud particles*, **lect. 6**.

[59] J. S. Shen and X. Cai, *Algorithm of Numerical Calculations on Mie Theory*, Progress in Electromagnetic Research Symposium, August 22-26, (2005), China.

[60] A. Habanyama, *Interaction of Germanium with PlatinumGroup Metals in Lateral Diffusion Couple*, PhD Thesis, (2004), University of Cape Town, South Africa.

[61] Veeco Metrology Group, *Scanning Probe Microscope Training Note Book.* di Digital Instruments, **Version 3.0**.